

Citation for published version:

Cole, JM, Cramer, AJ & Zeidler, A 2015, 'A topological analysis of void spaces in tungstate frameworks: assessing storage properties for the environmentally important guest molecules and ions: CO₂, UO₂, PuO₂, U, Pu, Sr²⁺, Cs⁺, CH₄, and H₂', ACS Sustainable Chemistry and Engineering , vol. 3, no. 9, pp. 2112-2129. <https://doi.org/10.1021/acssuschemeng.5b00369>

DOI:

[10.1021/acssuschemeng.5b00369](https://doi.org/10.1021/acssuschemeng.5b00369)

Publication date:

2015

Document Version

Peer reviewed version

[Link to publication](#)

University of Bath

General rights

Copyright and moral rights for the publications made accessible in the public portal are retained by the authors and/or other copyright owners and it is a condition of accessing publications that users recognise and abide by the legal requirements associated with these rights.

Take down policy

If you believe that this document breaches copyright please contact us providing details, and we will remove access to the work immediately and investigate your claim.

Article

A Topological Analysis of Void Spaces in Tungstate Frameworks: Assessing Storage Properties for the Environmentally Important Guest Molecules and Ions: CO₂, UO₂, PuO₂, U, Pu, Sr²⁺, Cs⁺, CH₄, and H₂

Jacqueline Manina Cole, Alisha Cramer, and Anita Zeidler

ACS Sustainable Chem. Eng., **Just Accepted Manuscript** • DOI:
10.1021/acssuschemeng.5b00369 • Publication Date (Web): 15 Jul 2015

Downloaded from <http://pubs.acs.org> on July 23, 2015

Just Accepted

“Just Accepted” manuscripts have been peer-reviewed and accepted for publication. They are posted online prior to technical editing, formatting for publication and author proofing. The American Chemical Society provides “Just Accepted” as a free service to the research community to expedite the dissemination of scientific material as soon as possible after acceptance. “Just Accepted” manuscripts appear in full in PDF format accompanied by an HTML abstract. “Just Accepted” manuscripts have been fully peer reviewed, but should not be considered the official version of record. They are accessible to all readers and citable by the Digital Object Identifier (DOI®). “Just Accepted” is an optional service offered to authors. Therefore, the “Just Accepted” Web site may not include all articles that will be published in the journal. After a manuscript is technically edited and formatted, it will be removed from the “Just Accepted” Web site and published as an ASAP article. Note that technical editing may introduce minor changes to the manuscript text and/or graphics which could affect content, and all legal disclaimers and ethical guidelines that apply to the journal pertain. ACS cannot be held responsible for errors or consequences arising from the use of information contained in these “Just Accepted” manuscripts.

1
2
3
4
5
6
7
8
9
10
11
12
13
14
15
16
17
18
19
20
21
22
23
24
25
26
27
28
29
30
31
32
33
34
35
36
37
38
39
40
41
42
43
44
45
46
47
48
49
50
51
52
53
54
55
56
57
58
59
60

A Topological Analysis of Void Spaces in Tungstate Frameworks: Assessing Storage Properties for the Environmentally Important Guest Molecules and Ions: CO₂, UO₂, PuO₂, U, Pu, Sr²⁺, Cs⁺, CH₄, and H₂

Jacqueline M. Cole,^{a,b,c} Alisha J. Cramer,^a Anita Zeidler^{c†}*

Cavendish Laboratory, Department of Physics, University of Cambridge, J. J. Thomson
Avenue, Cambridge, CB3 0HE. UK.

^b Argonne National Laboratory, 9700 S Cass Avenue, Argonne, IL 60439. USA.

^c Department of Chemistry, University of Cambridge, Lensfield Road, Cambridge, CB2
1EW. UK.

[†] Current address: Department of Physics, University of Bath, Bath, BA2 7AY. UK.

* Author for correspondence (E-mail: jmc61@cam.ac.uk)

Keywords: host-guest, tungstate, framework structure, energy fuel storage, CO₂ emissions,
nuclear waste storage

Abstract

The identification of inorganic materials, which are able to encapsulate environmentally important small molecules or ions *via* host-guest interactions, is crucial for the design and development of next-generation energy sources and for storing environmental waste. Especially sought after are molecular sponges with the ability to incorporate CO₂, gas pollutants, or nuclear waste materials such as UO₂ and PuO₂ oxides or U, Pu, Sr²⁺ or Cs⁺ ions. Porous framework structures promise very attractive prospects for applications in environmental technologies, if they are able to incorporate CH₄ for biogas energy applications, or to store H₂, which is important for fuel cells e.g. in the automotive industry. All of these applications should benefit from the host being resistant to extreme conditions such as heat, nuclear radiation, rapid gas expansion, or wear and tear from heavy gas cycling. As inorganic tungstates are well known for their thermal stability, and their rigid open-framework networks, the potential of Na₂O-Al₂O₃-WO₃ and Na₂O-WO₃ phases for such applications was evaluated. To this end, all known experimentally-determined crystal structures with the stoichiometric formula M_aM'_bW_cO_d (M = any element) are surveyed together with all corresponding theoretically calculated Na_aAl_bW_cO_d and Na_xW_yO_z structures that are statistically likely to form. Network descriptors that categorize these host structures are used to reveal topological patterns in the hosts, including the nature of porous cages which are able to accommodate a certain type of guest; this leads to the classification of preferential structure types for a given environmental storage application. Crystal structures of two new tungstates NaAlW₂O₈ (**1**) and NaAlW₃O₁₁ (**2**) and one updated structure determination of Na₂W₂O₇ (**3**) are also presented from in-house X-ray diffraction studies, and their potential merits for environmental applications are assessed against those of this larger

1
2
3 data-sourced survey. Overall, results show that tungstate structures with three-nodal
4
5 topologies are most frequently able to accommodate CH₄ or H₂, while CO₂ appears to be
6
7 captured by a wide range of nodal structure types. The computationally generated host
8
9 structures appear systematically smaller than the experimentally determined structures. For
10
11 the structures of 1 and 2, potential applications in nuclear waste storage seem feasible.
12
13
14

16 Introduction

18
19
20 For many years, porous materials have garnered considerable attention, owing to the wide
21
22 range of applications that they potentially offer. The removal of pollutants from industrial
23
24 waste,¹⁻³ the selective removal and storage of radioactive ions from nuclear waste,⁴⁻⁷ and the
25
26 storage of small molecules in alternative energy technologies⁸⁻¹⁰ illustrate just a few of many
27
28 possibilities. Currently, the focus of interest seems to be centered on organic-inorganic
29
30 hybrid materials, generally known as metal-organic frameworks (MOFs), as these can be
31
32 custom-tailored to a specific pore size.^{3,8,11-17} Thus, MOFs have already demonstrated their
33
34 potential as storage materials for alternative fuels such as CH₄ and H₂,^{8,15,17-19} as CO₂
35
36 reservoirs for pollution-control measures,^{3,20} or, more recently, for the potential uptake of
37
38 volatile organic compounds.^{21,22} The high level of success that MOFs have enjoyed sparked
39
40 a search for other types of molecular architectures, which could be employed for similar
41
42 tasks; this has led to the development of organic analogues of MOFs, of the so-called
43
44 covalent organic frameworks (COFs).²³ Like MOFs, COFs have already proven their
45
46 potential as storage materials for H₂, CH₄, CO₂, and N₂.^{9,10} However, for applications
47
48 involving harsher environmental pollutants, such as the storage of radioactive waste or
49
50 volatile organic compounds, purely inorganic materials continue to dominate in practice.<sup>1,2,4-
51
52
53
54
55
56
57
58
59
60</sup>

1
2
3 In order to determine the suitability of potential candidates for these types of applications, the
4 void spaces in their crystalline solid-state frameworks should be examined initially. After all,
5 only if the guest molecule can be accommodated in the host, are further considerations
6 appropriate. In the ongoing search for usable materials, data mining of structure databases
7 can provide a useful tool to identify potential candidates for the applications in hand. For
8 example, a study on Li⁺ migration maps²⁶ examined the structure of channels within lithium-
9 containing inorganic compounds, using Voronoi-Dirichlet partitioning that is implemented in
10 the crystallographic topological analysis program TOPOS.²⁷ That study identified 277 out of
11 2171 crystal structures which contained suitable conduction channels; 26 of these structures,
12 despite not being previously known as solid electrolytes, showed potential promise as ionic
13 conductors.
14
15
16
17
18
19
20
21
22
23
24
25
26
27
28
29

30 We herein propose to employ Voronoi-Dirichlet partitioning to investigate the void space
31 within cages of 3-dimensional tungstate-based extended framework structures in a similar
32 way, i.e. by using topological net descriptors for comparisons in order to conduct a void
33 space analysis for identifying possible host/guest combinations. To the best of our
34 knowledge, this represents the first topological analysis of a large survey of tungstate
35 structures, which are sourced from experimental and computational data. Experimental data
36 emanate from the Inorganic Crystal Structure Database (ICSD) and from in-house
37 crystallographic studies of three phases of Na₂O-WO₃. Computational data were obtained
38 from a structure prediction approach, determining all structures containing Na⁺, W⁶⁺ and O²⁻
39 ions with or without Al³⁺ ions, which are statistically likely to form based on ionic
40 substitution considerations of known related structures. The topological nets and void
41 volumes of all these crystal structures are determined and compared in order to assess their
42 potential as hosts in host/guest media with environmental applications.
43
44
45
46
47
48
49
50
51
52
53
54
55
56
57
58
59
60

1
2
3 In the context of nuclear waste storage applications, the UO_2 and PuO_2 oxides, U and Pu ions
4 of various oxidation states, and Sr^{2+} and Cs^+ ions are explored as possible guests, out of the
5 myriad of waste products found in nuclear waste. Waste from nuclear facilities, in the form
6 of spent nuclear fuel, is found predominantly in the form of uranium or plutonium oxides.²⁸
7
8 Furthermore, current efforts, especially among tungstates, are largely focused on
9 encapsulating radioactive waste via ion-exchange,^{4-7,24,29} making the containment of U and
10 Pu ions also important. Meanwhile, high activity fission product radionuclides Cs^+ and Sr^{2+}
11 provide an additional focus for storage development. Within waste streams from nuclear
12 reactors, ^{137}Cs and ^{90}Sr generate most of the thermal heat found in high level waste, and
13 combined with their relatively short half-lives (<50 years), processing these two elements
14 separately from the rest of the waste stream is both practical and beneficial.³⁰ In the context
15 of environmental waste associated with climate change, the encapsulation of CO_2 is evaluated
16 with a view to offset carbon emissions. Meanwhile, the possible inclusion of CH_4 and H_2
17 molecules is considered for alternative energy storage applications, which stand to deter
18 carbon emissions.
19
20
21
22
23
24
25
26
27
28
29
30
31
32
33
34
35
36
37
38
39

40 The diverse origins of the obtained data also provide the opportunity to make a general
41 comparison of experimentally determined against theoretically calculated structures for this
42 family of inorganic materials; and to establish a relative ranking of the likely use of three in-
43 house characterized subject materials $\text{Na}_a\text{Al}_b\text{W}_c\text{O}_d$ ($a = 1,2$; $b = 0,1$; $c = 2,3$; $d = 7,8,11$)
44 within this representative set of all statistically conceivable tungstate framework structures.
45
46
47
48
49
50

51
52 The overarching workflow associated with this topologically-generated data-mining study
53 that pair-wise matches host-guest volumes is illustrated in Figure 1.
54
55
56
57
58
59
60

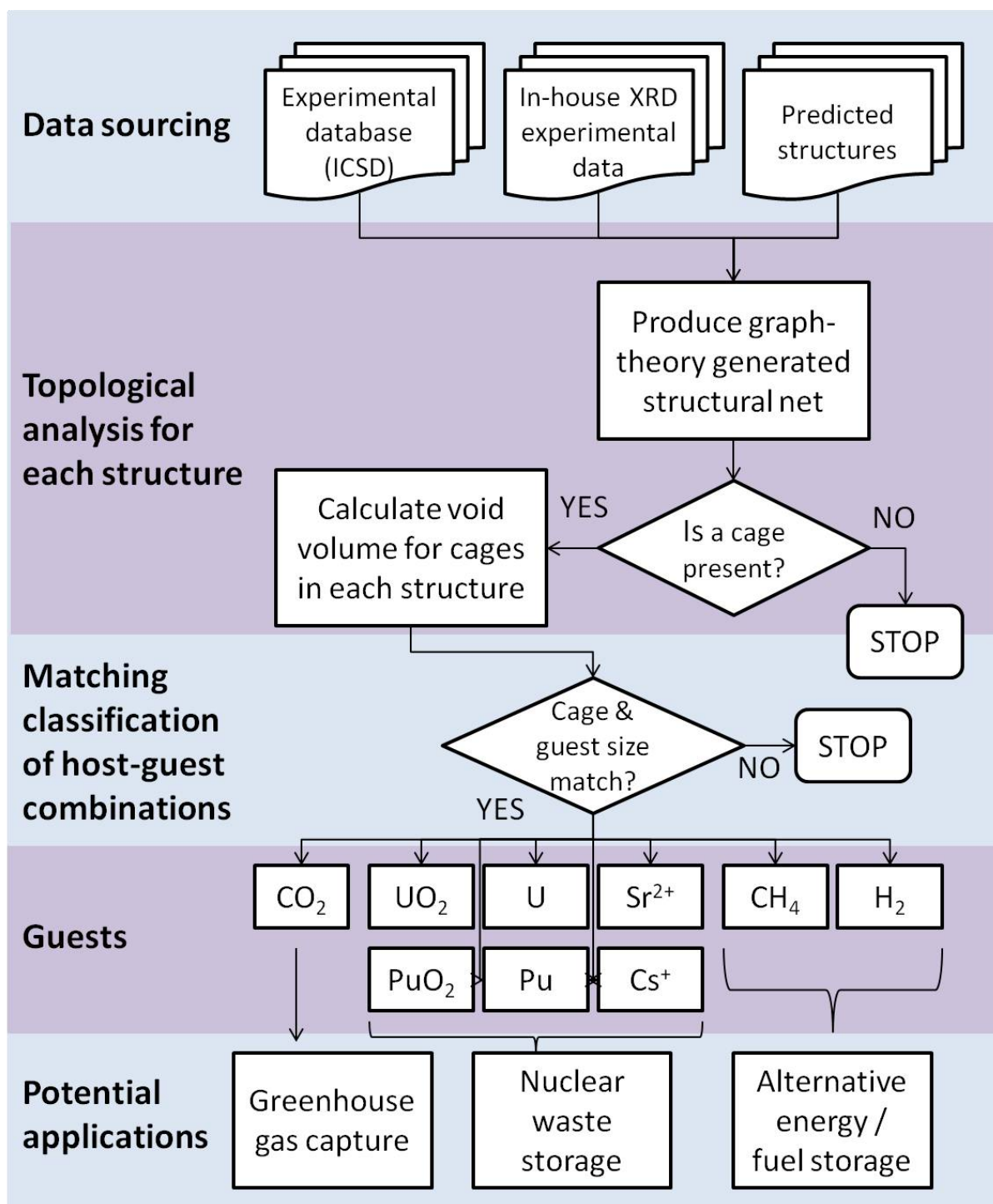


Figure 1. The overarching workflow for suiting host-guest pairs in tungstate-based structures with porous cages for guest inclusion.

Experimental and Computational Methods

Experimentally-derived crystal structure data of tungstate framework structures. Data for all 378 previously-reported crystal structures of ternary and quaternary tungstates of the general formulae $M_aW_yO_z$ or $M1_aM2_bW_yO_z$ ($M, M1, M2 = \text{any element}$) were extracted from the Inorganic Crystal Structure Database (ICSD). 284 of this total, which displayed structural frameworks that produce cages, were taken forward for full data analysis. Search parameter filters within the ICSD restricted structures to those containing W, O, and either 3 or 4 total element species. From the results, disordered structures, and those with partial occupancy in one or more of the atomic sites were manually excluded. The remaining list of structures was further refined by manually removing duplicates (structures with the same chemical formula, and spacegroup); among duplicate structures, those with the lowest R1 factor were kept.

In-house provision of crystal structure data: sample preparation and characterization of three Na₂O-Al₂O₃-WO₃ and Na₂O-WO₃ phases. Samples were prepared as previously described elsewhere.³¹ The crystal structures of two new compounds NaAlW₂O₈ (**1**) and NaAlW₃O₁₁ (**2**) were determined by single crystal X-ray diffraction. Furthermore, the crystal structure of Na₂W₂O₇ (**3**), was determined at low temperature ($T = 180(2) \text{ K}$), affording an improved structural model on the previously reported room-temperature structure.³²

Suitable single crystals were mounted onto glass fibers using perfluoropolyether oil. Diffraction data for (**1**) were collected on a Nonius Kappa CCD diffractometer, equipped with a monochromatic Mo-K α ($\lambda = 0.71073 \text{ \AA}$) X-ray source and an Oxford Cryosystems Cryostream open-flow N₂ cooling device. Cell parameters were refined against data from all regions of reciprocal space using HKLScalepack.³³ Data reduction employed HKLDenzo and Scalepack,³³ while data sets were corrected for Lorentz and polarisation effects, as well

1
2
3 as for absorption using SORTAV.³⁴ Diffraction data for (2) and (3) were collected on a
4
5 Rigaku Saturn 724+ CCD diffractometer, equipped with a monochromatic Mo-K α ($\lambda =$
6
7 0.71073 Å) X-ray source, SHINE Optics, and an Oxford Cryosystems CryostreamPlus open-
8
9 flow N₂ cooling device. Cell refinement, data collection, and data reduction were carried out
10
11 with Rigaku CrystalClear-SM Expert 2.0 software,³⁵ whereas absorption correction was
12
13 implemented using ABSCOR.³⁶
14
15
16

17
18 All structures were solved with direct methods and refined by full-matrix least squares
19
20 methods on F2 using SHELXL-97.³⁷ Full details for crystal, data collection and refinement
21
22 parameters are provided in the Supporting Information.
23
24

25
26 A few specific technical notes about the structure solution and refinement of (1)-(3) are worth
27
28 mentioning. Owing to its pseudo-orthorhombic unit cell, the structure of (1) displays a small,
29
30 but nevertheless distinct, pseudo-merohedral twin component, resulting in a fractional twin
31
32 contribution of 0.16(3)%. Compound (2) displays significant structural disorder, to the
33
34 extent that its elemental and stoichiometric composition needed verification from energy-
35
36 dispersive X-ray (EDX) analysis to aid crystal structure determination. The EDX experiment
37
38 employed a Zeiss Cross Beam scanning electron microscope, which afforded the following
39
40 elemental proportions: Na = 5.47%; Al = 5.13%; W = 15.54%; O = 65.62%. A residual
41
42 8.34% arising from a contribution of carbon was attributed to surface contamination. These
43
44 results were particularly important in checking that the compound contained Al, rather than
45
46 Cr, which could have substituted Al as a reaction contaminant. The structure of (3) matches
47
48 the previously determined crystal structure of this material,³² albeit with improved refinement
49
50 statistics and different thermal parameters owing to the low-temperature data collection
51
52 nature of this new study.
53
54
55
56
57
58
59
60

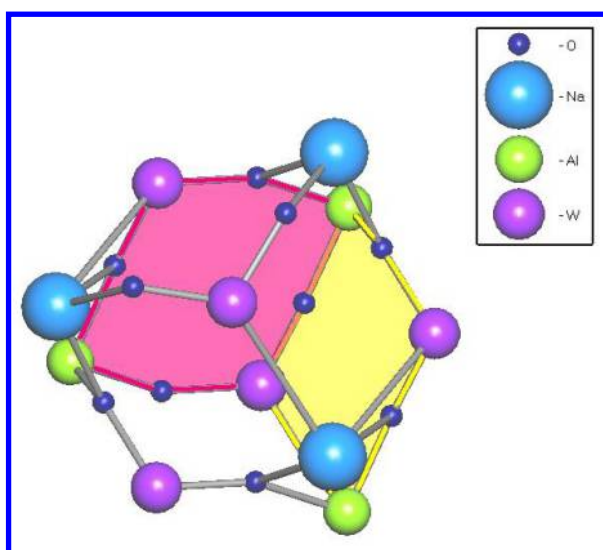
1
2
3 **Theoretically calculated predictions for tungstate structures.** All hypothetically possible
4 crystal structures containing any statistically conceivable combination of W, P, Al and O ions
5 were generated computationally by using previously described methods.³⁸ The possibility of
6 individual crystal structures was based on the statistical probability for existing structural
7 motifs in the Inorganic Crystal Structure Database (ICSD) to be transmuted into tungstates
8 via ionic substitution. The probability of ionic substitution was determined via a reference
9 pair correlation matrix of various ion combinations, where each matrix element, g_{AB} ,
10 represents the probability of ionic substitution between a given pair of ions A and B. This
11 probability has been pre-calculated by enumerating the relative number of crystal structure
12 examples in the ICSD, which differ only in the ions A and B. This method accordingly
13 assesses the relative ease by which a given ion can fit into the crystallographically equivalent
14 site of another ion. Values for g_{AB} were therefore derived from a pre-trained reference
15 library of structural homologues of A and B. While this was not part of the probabilistic
16 calculation, it is hardly surprising that two ions of similar size, chemical properties (e.g. from
17 the same group in the periodic table), and/or identical charge tend to have higher g_{AB} values,
18 since substitution for each proceeds more readily. For example, when $A = W^{6+}$, the highest
19 g_{AB} value was obtained for $B = Mo^{6+}$, whereas when $A = Al^{3+}$, large g_{AB} values were
20 obtained for $B = Cr^{3+}$, Fe^{3+} , In^{3+} , or Ga^{3+} .
21
22
23
24
25
26
27
28
29
30
31
32
33
34
35
36
37
38
39
40
41
42
43
44
45

46
47 Only charge-balanced crystal structures, and those not already in the ICSD, were considered
48 in the theoretical structure prediction results. In total, 196 hypothetical tungstate structures of
49 the general formula $Na_mW_nAl_oO_p$ were generated computationally. 43 of these calculated
50 structures were taken forward for full void-space analysis since only these produced cages,
51 which are of course necessary for hosting guest molecules or ions.
52
53
54
55
56
57
58
59

60 **Topological Analysis**

1
2
3 **TOPOS methods.** All selected tungstate structures were assessed for their potential for
4 hosting the subject guest molecules and ions, using the crystallographic topological analysis
5 program package, TOPOS 4.0 Professional.²⁷ This enabled the topological classification of
6 each tungstate structure, and the determination and analysis of the void space residing within
7 its framework.
8
9
10
11
12
13
14
15

16 This analysis was accomplished by first defining the topological net of each structure using
17 the ADS module in TOPOS. Such nets were identified using graph theory to calculate a map
18 of the circuits contained therein by viewing all atoms as nodes, and all bonds as edges,
19 thereby ascertaining the geometrical patterns in the crystal structure. These nets were then
20 categorized as n-nodal in the presence of n different kinds of inequivalent vertices in the net.
21 The net may contain tiles, defined as generalized polyhedra (cages) which have at least two
22 edges incident upon each vertex and two faces incident upon each edge.^{39,40} These tiles are
23 described according to how many faces a given tile possesses with each face being defined by
24 its m-membered rings. This nodal/tiling topological representation is illustrated in Figure 2,
25 using the example of (1). The full classification of a net is based on several conventional
26 descriptors, which may be used to search the TOPOS Topological Database (TTD) for the
27 topological type of the net (for a full explanation and list of these descriptors see^{41,42}).
28
29
30
31
32
33
34
35
36
37
38
39
40
41
42
43



1
2
3 **Figure 2.** A 22/11 net using (1) as the example: $[3^2.4^3.6.7^2.8^3]$ tile, whereby 22/11
4 denominates the total number of nodes/tiles; $[3^2.4^3.6.7^2.8^3]$ indicates the presence of 2 faces
5 consisting of 3-membered rings, 3 faces consisting of 4-membered rings, 1 face consisting of
6 a 6-membered ring, 2 faces consisting of 7-membered rings (e.g. yellow plane), and 3 faces
7 consisting of 8-membered rings (e.g. pink plane).
8
9
10
11
12
13
14
15
16
17

18 Void space analysis was then accomplished via a two-step process: the determination of all
19 cages found within each structure, prior to calculating the void space volume within each
20 cage using Voronoi-Dirichlet polyhedra (VDP). Thus, a comparison basis for the cavity
21 volumes in each structure was established in the first step. Cages can be found from the net
22 topology, and were determined using the ADS module in TOPOS. For three-dimensional
23 periodic framework structures, the circuits formed by the atoms and bonds can be combined
24 to form generalized polyhedra that are topologically equivalent to spheres. For an in-depth
25 discussion of cages and tiling, see ^{39,43}.
26
27
28
29
30
31
32
33
34
35
36
37

38 The second step of void-space analysis comprises the calculation of a Voronoi-Dirichlet
39 partition of the crystal space for each cage, using the Dirichlet module in TOPOS to construct
40 the VDP for all independent framework atoms. From this partition, the location and size of
41 voids were obtained by placing a node at the intersection of four or more VDP vertices.
42 Subsequently, the Voronoi-Dirichlet partition was reconstructed taking the void nodes into
43 account, which resulted in a map of the void space of the structure. In order to analyze the
44 cavity size within individual cages, the cages were isolated and void nodes were generated
45 from the atoms forming the cage. Subsequently, VDP were generated for these void nodes,
46 from which their volumes were calculated.
47
48
49
50
51
52
53
54
55
56
57
58
59
60

1
2
3 **Guest volume determination.** The intrinsic volumes of the guest molecules or ions were
4 estimated in three different ways. For individual ions (U, Pu, Cs⁺, Sr²⁺), radii of 1.75 Å, 1.75
5 Å, 2.60 Å, and 2.00 Å, respectively, were obtained from the Slater radii⁴⁴ database in
6 TOPOS. Subsequently, these radii were employed to calculate spherical volumes. The
7 volumes of the UO₂ and PuO₂ oxides were extracted from their previously reported
8 experimentally-determined crystal structures, as sourced from the ICSD. Owing to the three
9 dimensional frameworks formed by UO₂ and PuO₂ crystal structures, volume determination
10 of discrete molecules was unfeasible. Hence, the volumes of a single U or Pu, and the eight
11 valence-bonded oxygens for each were determined for chosen samples of UO₂⁴⁵ and PuO₂,⁴⁶
12 respectively.
13
14
15
16
17
18
19
20
21
22
23
24
25
26
27

28 Volumes for small guest molecules, such as CO₂, CH₄, and H₂ were established based on
29 previously published kinetic diameters (3.3 Å, 3.8 Å, and 2.89 Å, respectively), from which
30 spherical volumes were calculated. As the kinetic diameter represents only the smallest
31 dimension of a given molecule, the calculated spherical volumes are necessarily the smallest
32 possible volume for that molecule, and there is no consideration of the shape of the molecule
33 in this calculation. This is acceptable as long as an upper bound of guest volumes within a
34 cage can be set to provide the necessary latitude to allow for the molecule size to be greater in
35 its other dimensions.
36
37
38
39
40
41
42
43
44
45
46
47

48 The resulting volumes for all guest molecules and ions were rounded up to the nearest whole
49 integer, in order to establish the lowest bound of the desired cage size. An upper bound was
50 set 4 Å³ above this lower bound, which should allow the guest some spatial flexibility,
51 without allowing more than one guest within a single cage. An exception to this is H₂, where
52 a maximum of two molecules may fit in a cage at the upper limit.
53
54
55
56
57
58
59
60

Results and Discussion

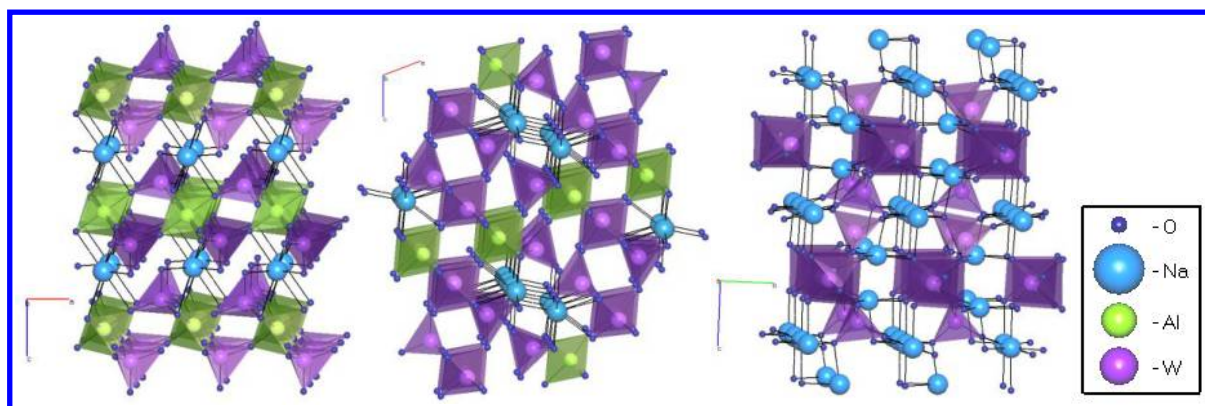
New Crystal Structures

NaAlW₂O₈ (1). The W-Al network in (1) consists of 4-membered rings with alternating octahedrally-coordinated Al and tetrahedrally-coordinated W atoms, whereby Na atoms occupy the space between rings (Figure 3 (left)). One might naturally suppose that the framework of (1) would be isostructural to the previously reported MM'W₂O₈ (M, M' = metal) crystal structures, NaCrW₂O₈ and NaInW₂O₈, which form layers of polyhedra in the order Na, W, In/Cr, W, Na yielding a 2-nodal net of the α -PbO₂ topological type.⁴⁷ However, it is not; instead, (1) turns out to be isomorphic with the molybdate compound, NaAlMo₂O₈,⁴⁸ manifesting coordination polyhedra that form a 6-nodal topological net.

All atoms in the structural framework of (1) lie on general positions with the exception of the Al, which is located on an inversion centre. The observed W \cdots O bond lengths range from 1.743 (5) - 1.806 (4) Å, whereas the Al \cdots O bond lengths range from 1.874 (4) - 1.891 (4) Å, and the Na \cdots O bond lengths span a range from 2.367 (4) - 2.924 (4) Å.

NaAlW₃O₁₁ (2). (2) features two tetrahedral and one octahedrally coordinated W, as well as one octahedrally-coordinated Al, forming the main part of the network, with Na atoms occupying sites inside the framework. The W-Al network adopts a (3,6)-coordinated 2-nodal net which corresponds to a standard topological type, 3,6T36. This network consists of 4-membered rings of alternating octahedrally-coordinated W and Al, which are connected *via* their apexes to 4-membered rings of alternating octahedrally-coordinated Al and tetrahedrally-coordinated W ions (Figure 3 (middle)). Inclusion of the Na ions results in the formation of a 9-nodal net.

1
2
3 $\text{Na}_2\text{W}_2\text{O}_7$ (3). In contrast to (1) and (2), (3) lacks any Al ions, and so the coordination sites
4
5 of its structure contain exclusively octa- and tetrahedrally coordinated W ions (Figure 3
6
7 (right)). Topologically, this can be classified as a 9-nodal net. The W network contains long
8
9 chains of octahedrally-coordinated W, wherein the tetrahedrally-coordinated W ions adopt
10
11 alternating positions on both sides of the chain. The Na ions occupy coordination sites
12
13 between these chains, coordinating to the terminal oxygens of the tetra- and octahedrally-
14
15 coordinated W ions.
16
17
18
19



20
21
22
23
24
25
26
27
28
29
30
31
32
33 **Figure 3.** The crystal structures of (1) and (2) viewed down the b-axis (left and middle); and
34
35 (3) viewed down the a-axis (right).
36
37

38
39 **Guest/host comparisons for environmental applications.** In total, 577 crystal structures of
40
41 tungstate-based extended frameworks were surveyed for their prospects as host materials for
42
43 the environmentally important guest molecules or ions: CO_2 , UO_2 , PuO_2 , U, Pu, Sr^{2+} , Cs^+ ,
44
45 CH_4 , and H_2 . 196 were hypothetical crystal structures generated from computational
46
47 predictions, while the other 381 were sourced from (378) previously reported or (3) in-house
48
49 data from diffraction experiments. Of these, 284 previously reported crystal structures, 43
50
51 hypothetical structures, and the three in-house determined structures produced topological
52
53 tilings; the ten largest cages in these 331 tilings were subsequently identified and their
54
55 corresponding void volumes calculated (see Supporting Information). Possible guest-host
56
57
58
59
60

1
2
3 matches were then assessed by comparing these void space volumes of the framework
4
5 structures against the size of each subject guest molecule or ion.
6
7

8
9 **CO₂ capture.** The optimal cavity size for the incorporation of CO₂ was determined using its
10 kinetic diameter of 3.3 Å,⁴⁹ providing a target volume of 19 – 23 Å³. The structural analysis
11 identified 52 previously reported experimentally-determined crystal structures containing 60
12 cages with appropriate void space volumes. Of these, 47 structures had one suitable cage
13 volume per structure; the remaining 5 structures contained two or more suitable cages
14 (hereafter designated as ‘multiple cages’) per structure. The subsequent breakdown of all
15 suitable cages by type found that 16 cages suited for hosting a guest were found to be the
16 largest (primary, 1°) cage formed by the structure, whereas in 17 of the cages it was the
17 secondary (2°) cage with suitable void space, and 27 cages of interest were tertiary (3°) or
18 higher (3°+). Furthermore, five of the compounds contained at least two cages suitable for
19 CO₂ storage. Among the calculated structures, a total of 13 structures were found to contain
20 21 suitable cages (1 x 1°; 3 x 2°; 17 x 3°+), with seven of the structures exhibiting multiple
21 cages. None of the in-house experimentally-determined crystal structures (1)-(3) were found
22 to contain cages suitable for CO₂ containment. Figure 4 summarizes these statistics, while
23 representative example structures from the most common (5- and 6-nodal) nets that
24 demonstrate capacity to host CO₂ are displayed in Figure 5.
25
26
27
28
29
30
31
32
33
34
35
36
37
38
39
40
41
42
43
44
45
46
47
48
49
50
51
52
53
54
55
56
57
58
59
60

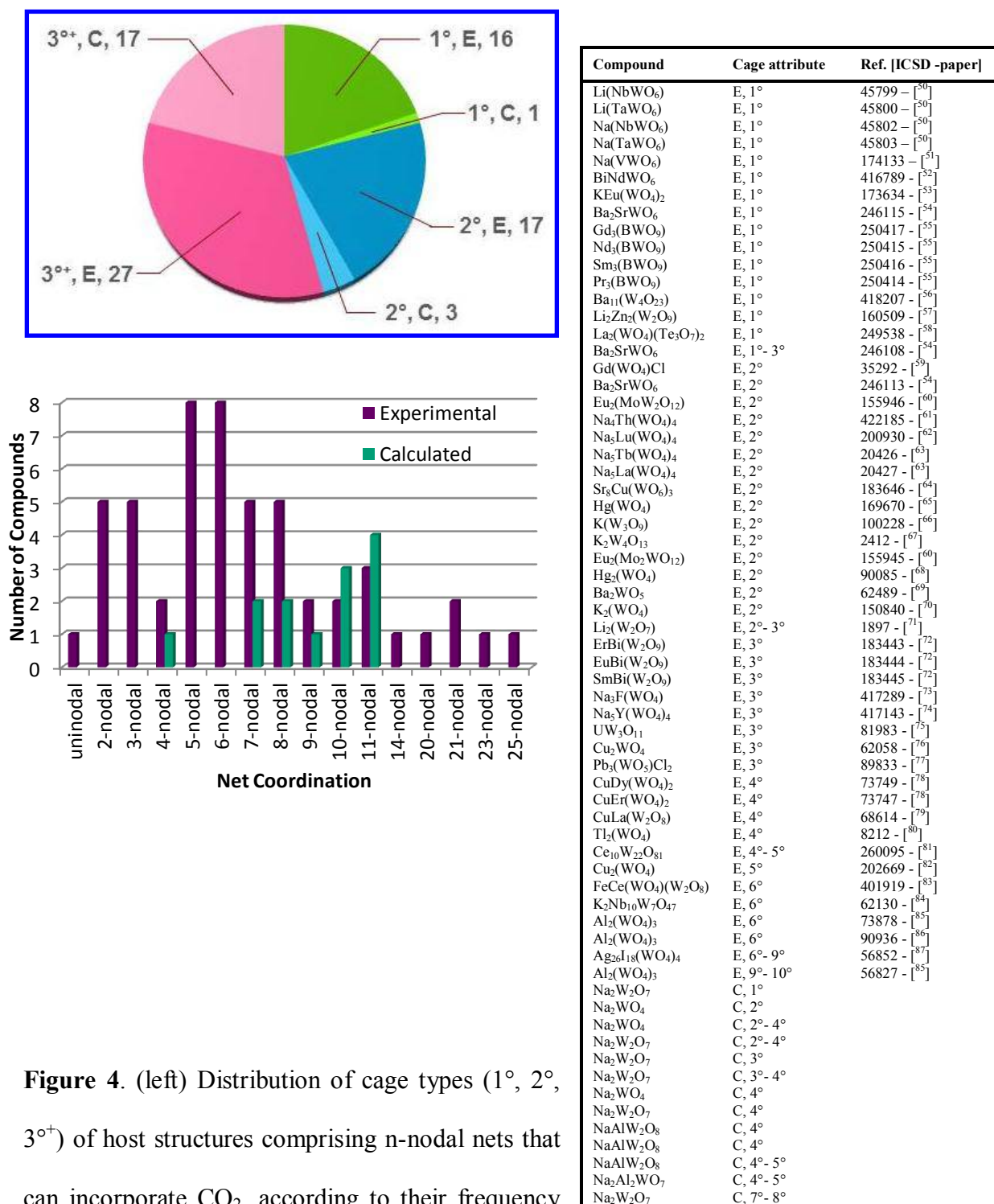


Figure 4. (left) Distribution of cage types (1°, 2°, 3°) of host structures comprising n-nodal nets that can incorporate CO₂, according to their frequency observed in experimental (E) and calculated (C) crystal structures; (right) a list of their associated compound identifiers (ICSD number and reference citation).

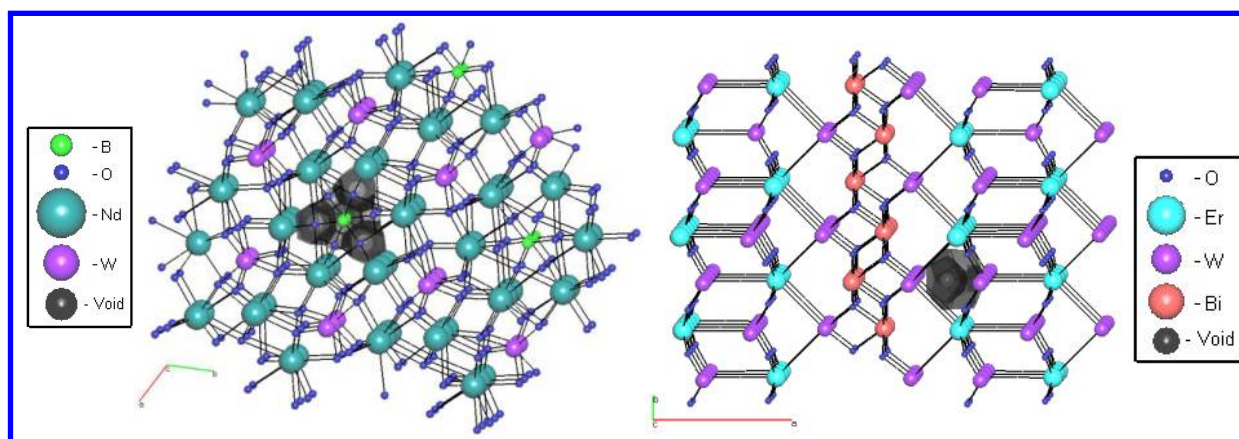


Figure 5. Representative example host framework structures from the two most common types of n -nodal nets whose cages have suitable void space volumes (black/grey) to accommodate CO_2 molecules: 5-nodal (left; $\text{Nd}_3(\text{BWO}_9)$ [ICSD ref. 250415 – [55]]) and 6-nodal (right; $\text{ErBi}(\text{W}_2\text{O}_9)$ [ICSD ref. 183443 – [72]]).

Nuclear waste storage.

UO_2 . The potential inclusion of UO_2 was examined on the basis of the TOPOS-generated VDP volume for a single cube of 8-coordinated U from the UO_2 crystal structure (ICSD reference no. 246851 – [45]; space group $Fm-3m$; unit cell $a = 5.468\text{\AA}$). This produced a void-space volume of 63.09\AA^3 which gave a targeted void space volume of $64 - 68\text{\AA}^3$. This range identified only two suitable cages within previously reported structures, one within predicted structures, and two within the in-house structures ((1) and (2)), as seen in Figure 6. All structures contained only 1° cages. With such a limited sampling, there is no net type that is more common than any other for hosting UO_2 . As such, (1) will serve as the representative example structure with a 6-nodal net, shown in Figure 7.

Compound	Cage attribute	Ref. [ICSD paper]	-
			17

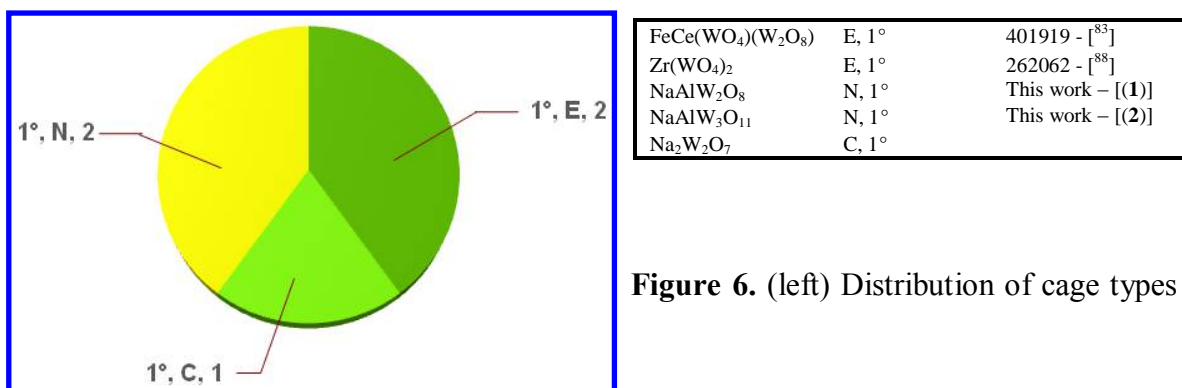
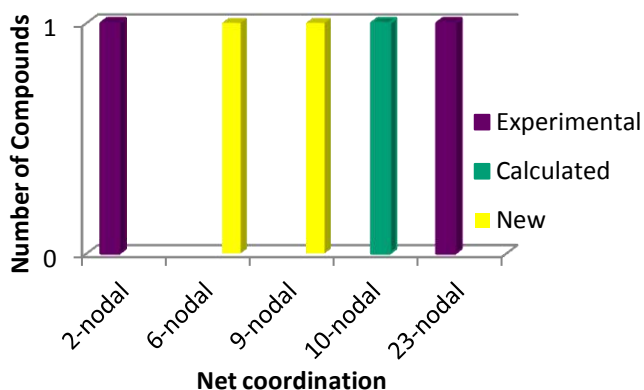
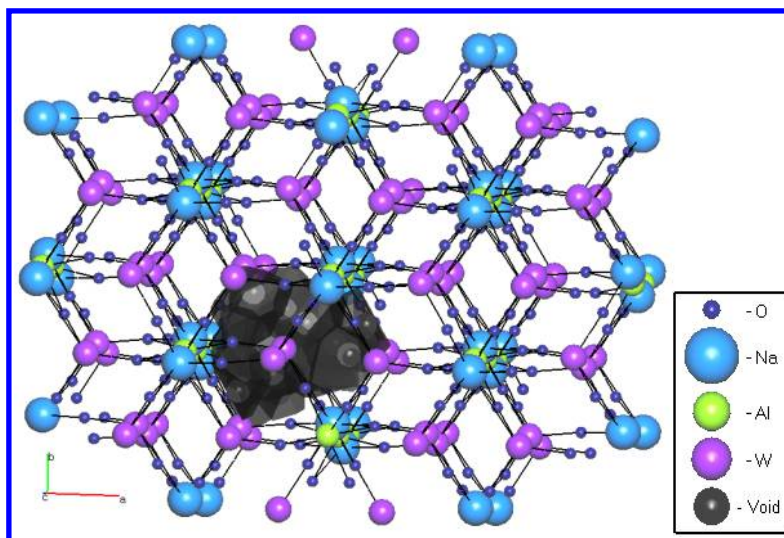


Figure 6. (left) Distribution of cage types



(1°) of host structures comprising n-nodal nets that can incorporate UO₂, according to their frequency observed in previously reported (E) or newly-determined (N) experimental and calculated (C) crystal structures; (right) a list of their associated compound identifiers (ICSD number and reference citation).

**Figure 7. A**

representative example of a crystal structure (of NaAlW_2O_8 [this work (1)]) bearing a ($n = 6$) n -nodal net that contains cages with suitable void space volumes (black/grey) to accommodate UO_2 .

PuO_2 . Determination of the PuO_2 volume followed the same general pattern as for UO_2 . The VDP volume of a single cube of 8-coordinated Pu was obtained from TOPOS using the PuO_2 crystal structure (ICSD reference no. 55456 – [⁴⁶], space group Fm-3m, unit cell $a = 5.3982$ Å). This afforded a target void-space volume range of $61 - 65$ Å³. The topological analysis identified eight suitable cages amongst seven previously reported crystal structures: $6 \times 1^\circ$; $2 \times 2^\circ$, with one structure containing both 1° and 2° cages of a suitable size; a 3° cage in one predicted structure, and a 1° cage in the new structure, (2). Figure 8 summarizes these statistics. Figure 9 provides a representative example of a tungstate-based framework structure belonging to the most common type of n -nodal net ($n = 9$) that bears a cage suitable for PuO_2 containment.

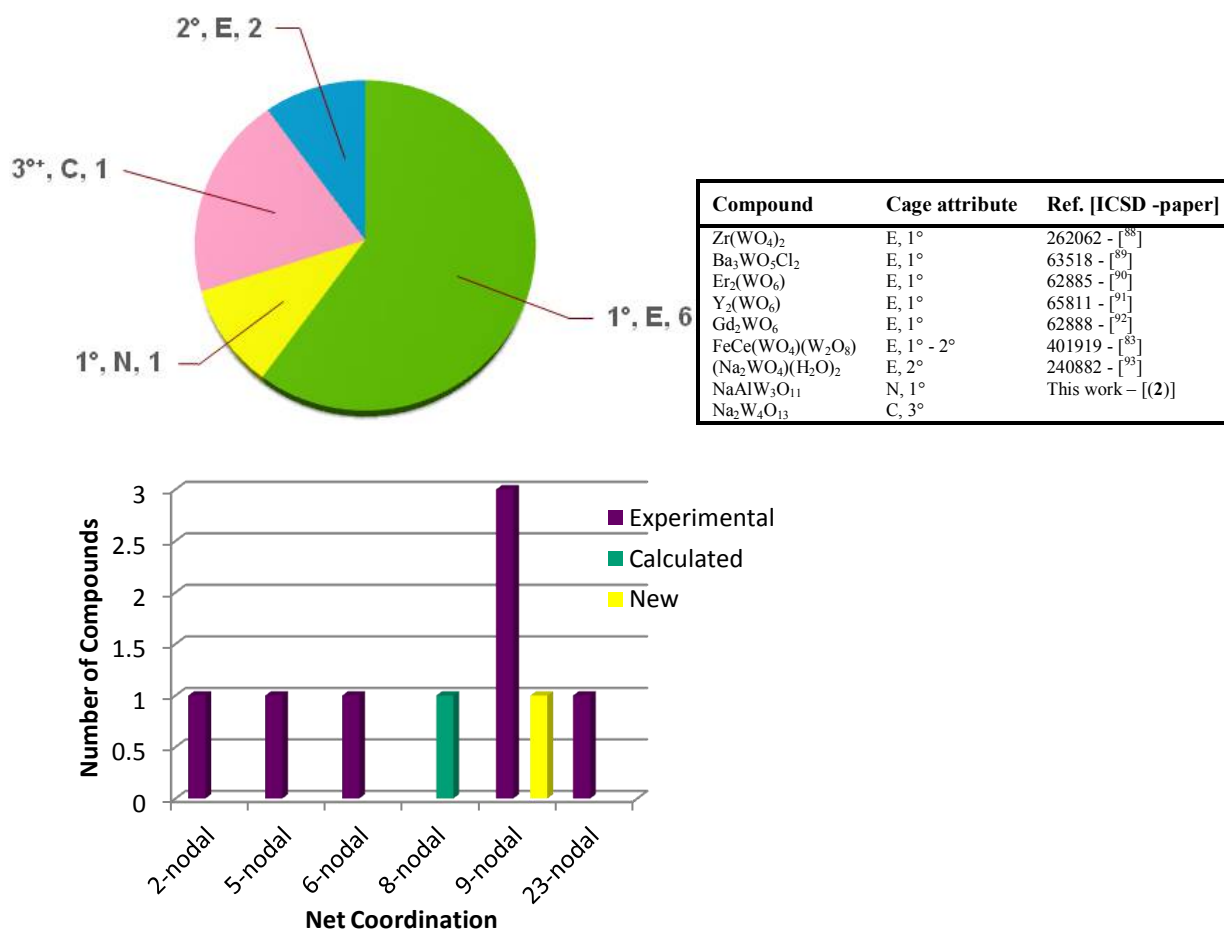
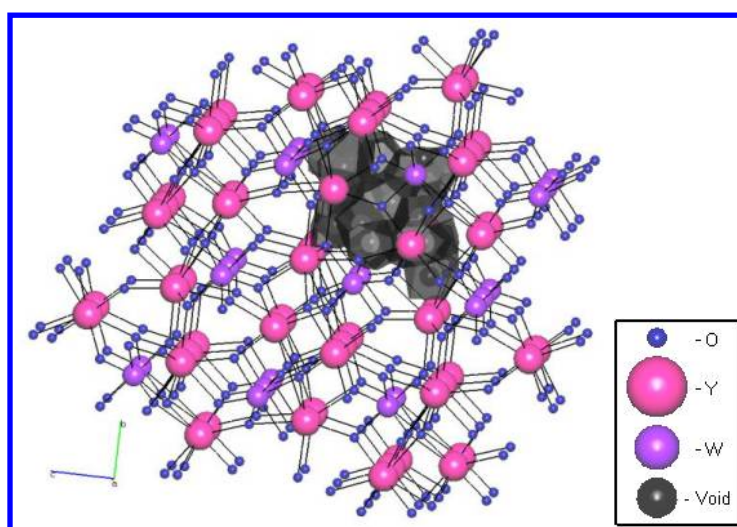
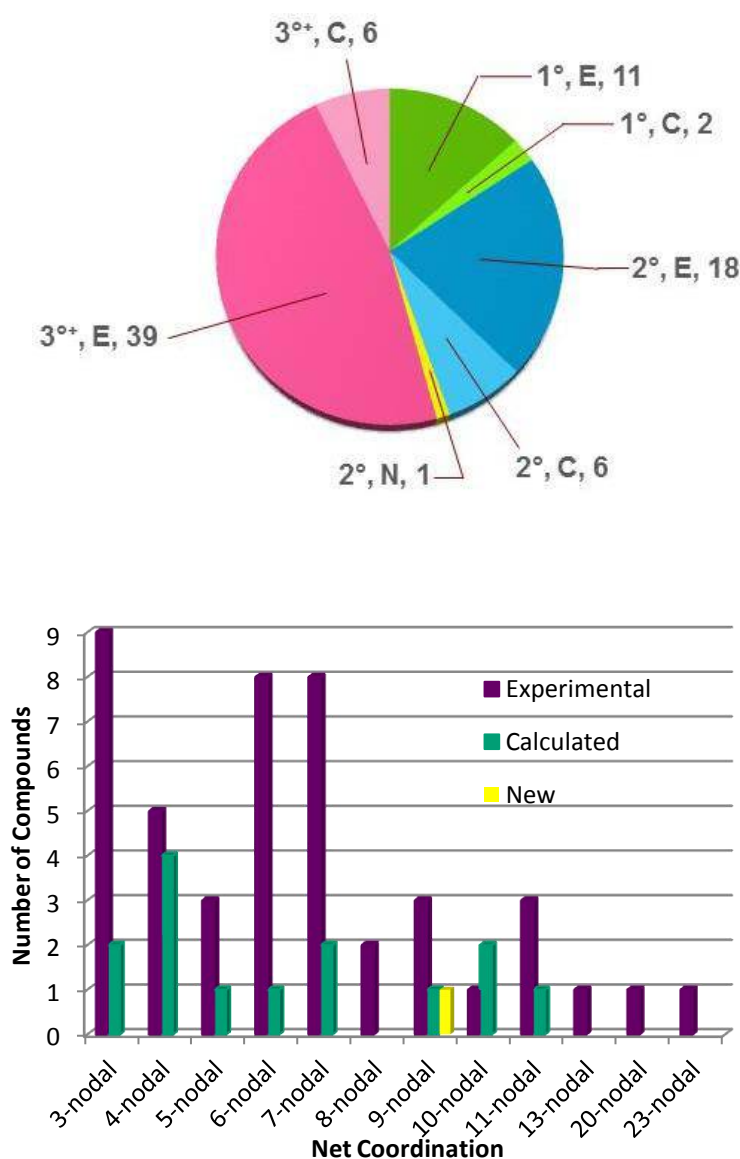


Figure 8. (left) Distribution of cage types (1°, 2°, 3°) of host structures comprising n-nodal nets that can incorporate PuO₂, according to their frequency observed in previously reported (E) or newly-determined (N) experimental and calculated (C) crystal structures; (right) a list of their associated compound identifiers (ICSD number and reference citation).



1
2
3 **Figure 9.** A representative example of a crystal structure (of $Y_2(WO_6)$ [ICSD ref. 65811 –
4 $[^{91}]$]) bearing the most common ($n = 9$) n-nodal net that contains cages with suitable void
5 space volumes (black/grey) to accommodate PuO_2 .
6
7
8
9

10
11 **U or Pu ions.** Although it would be more accurate to investigate ions, differences in reactor
12 type, reprocessing, and waste management techniques can result in different states of a given
13 ion within the waste material. In natural water-rock systems, Pu has four oxidation states (3^+ ,
14 4^+ , 5^+ , 6^+), while U can often be found as U^{4+} or U^{6+} ,⁹⁴ as such, it was decided to use the
15 atomic radii for these elements since this represents the largest volume that would potentially
16 be necessary for encapsulation. U and Pu atoms presented the same Slater radii⁴⁴ listings in
17 TOPOS, and so were considered together in terms of finding suitable host structures to
18 contain them. The associated target void-space volumes were 23-27 \AA^3 . This resulted in the
19 selection of 45 previously reported crystal structures that feature 68 suitable cages (11 x 1° ;
20 18 x 2° ; 39 x 3° ; 13 x multiple cages); 13 predicted structures (2 x 1° ; 6 x 2° ; 6 x 3°) one of
21 which contains both a 2° and 3° cage; and one newly-determined crystal structure, ((**3**),
22 bearing a 2° cage). Figure 10 displays these results. A representative example structure,
23 bearing the most common type of n-nodal net ($n = 3$) whose cages appear to be able to host U
24 or Pu ions, is presented in Figure 11.
25
26
27
28
29
30
31
32
33
34
35
36
37
38
39
40
41
42
43
44
45
46
47
48
49
50
51
52
53
54
55
56
57
58
59
60



Compound	Cage attribute	Ref. [ICSD - paper]
KLu(WO ₄) ₂	E, 1°	172510 - [95]
KYb(WO ₄) ₂	E, 1°	280877 - [96]
KEr(WO ₄) ₂	E, 1°	157832 - [97]
KY(WO ₄) ₂	E, 1°	411285 - [98]
KHo(WO ₄) ₂	E, 1°	182626 - [99]
Sr ₂ (CuWO ₆)	E, 1°	99303 - [100]
Li ₂ Cu(WO ₄) ₂	E, 1°	92854 - [101]
Li ₂ Ni(WO ₄) ₂	E, 1°	92853 - [101]
Li ₂ Co(WO ₄) ₂	E, 1°	92852 - [101]
Ce ₁₀ W ₂₂ O ₈₁	E, 1° - 3°	260095 - [81]
Bi ₂ WO ₆	E, 1° - 3°	171328 - [102]
Dy ₂ (WO ₄) ₃	E, 2°	98102 - [103]
Eu ₂ (WO ₄) ₃	E, 2°	15877 - [104]
Pb ₃ (WO ₃)Cl ₂	E, 2°	89833 - [77]
Pr ₃ (WO ₆)Cl ₃	E, 2°	20626 - [105]
La ₃ WO ₆ Cl ₃	E, 2°	35595 - [106]
Rb ₁₂ (Nb ₃₀ W ₃ O ₉₀)	E, 2°	1505 - [107]
LiY(W ₂ O ₈)	E, 2°	156989 - [108]
ErBi(W ₂ O ₉)	E, 2°	183443 - [72]
EuBi(W ₂ O ₉)	E, 2°	183444 - [72]
SmBi(W ₂ O ₉)	E, 2°	183445 - [72]
Ca ₄ (Al ₆ O ₁₂)(WO ₄)	E, 2°	28481 - [109]
Na ₂ (W ₂ O ₇)	E, 2°	1883 - [32]
Sr ₄ (Al ₆ O ₁₂)(WO ₄)	E, 2°	28483 - [109]
UW ₃ O ₁₁	E, 2°	81983 - [75]
Ba ₃ WO ₅ Cl ₂	E, 2° - 3°	63518 - [89]
CuSm(W ₂ O ₈)	E, 2° - 3°	68615 - [79]
CuGd(W ₂ O ₈)	E, 3°	75006 - [110]
LiPr(WO ₄) ₂	E, 3°	200520 - [111]
CuDy ₅ (WO ₄) ₈	E, 3°	380067 - [112]
Tl ₂ (WO ₄)	E, 3°	8212 - [80]
Rb ₂ (WO ₄)	E, 3°	183200 - [113]
Rb(NbW ₂ O ₉)	E, 3°	246143 - [114]
Al ₂ (WO ₄) ₃	E, 3° - 5°	73878 - [85]
Al ₂ (WO ₄) ₃	E, 3° - 5°	90936 - [86]
FeCe(WO ₄)(W ₂ O ₈)	E, 4° - 5°	401919 - [83]
U(WO ₄)	E, 4° - 5°	2285 - [115]
Al ₂ (WO ₄) ₃	E, 4° - 8°	56827 - [85]
Li ₂ (WO ₄)	E, 5° - 6°	160721 - [116]
Li ₂ (WO ₄)	E, 5° - 6°	15395 - [117]
Sc ₂ (WO ₄) ₃	E, 6°	28467 - [118]
In ₂ (WO ₄) ₃	E, 6°	99606 - [119]
Ba ₂ P ₈ W ₃₂ O ₁₁₂	E, 7° - 9°	202484 - [120]
Al ₂ (WO ₄) ₃	E, 8° - 10°	73879 - [85]
(Na ₂ WO ₄)(H ₂ O) ₂	E, 9°	240882 - [93]
Na ₂ W ₂ O ₇	N, 2°	This work - [(3)]
Na ₂ WO ₄	C, 1°	
Na ₂ WO ₄	C, 1°	
Na ₄ WO ₅	C, 2°	
Na ₂ WO ₄	C, 2°	
Na ₂ W ₂ O ₇	C, 2°	
Na ₂ W ₂ O ₇	C, 2°	
Na ₂ W ₂ O ₇	C, 2°	
Na ₂ W ₂ O ₇	C, 2°	
Na ₂ Al ₂ WO ₇	C, 2° - 3°	
Na ₂ WO ₄	C, 3°	
Na ₂ W ₂ O ₇	C, 3°	
Na ₂ W ₂ O ₇	C, 3°	
NaAlW ₂ O ₈	C, 3°	
Na ₂ W ₂ O ₇	C, 8°	

Figure 10. (left) Distribution of cage types (1°, 2°, 3⁺) of host structures comprising n-nodal nets that can incorporate U or Pu ions, according to their frequency observed in previously reported (E) or newly-determined (N) experimental and calculated (C) crystal structures; (right) a list of their associated compound identifiers (ICSD number and reference citation).

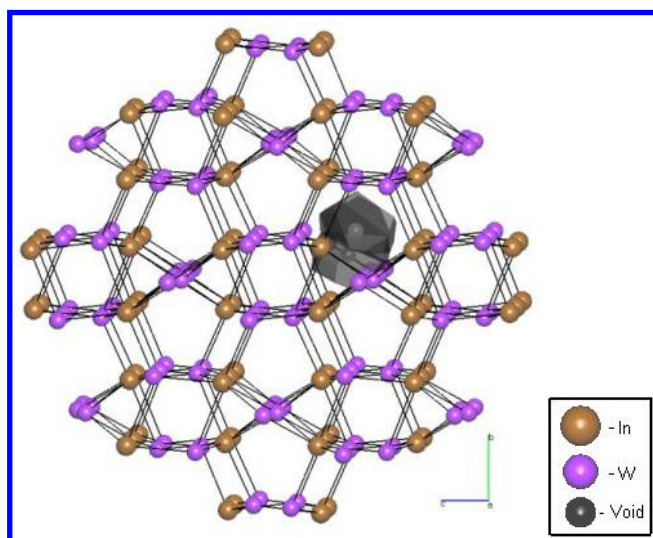


Figure 11. A representative example of a crystal structure (of $\text{In}_2(\text{WO}_4)_3$ [ICSD ref. 99606 – $[\text{119}]]$) featuring the most common ($n = 3$) n -nodal net that bears cages with suitable void space volumes (black/grey) to contain U or Pu ions.

Cs⁺ ions. The occupational volume for Cs⁺ ions was also obtained from the Slater radius⁴⁴ parameter in TOPOS, resulting in a target void-space volume of 74 – 78 Å³. For this range, suitable cages in four previously reported (3 x 1°; 1 x 2°) and four predicted (3 x 1°; 1 x 2°) structures were identified (Figure 12). Figure 13 illustrates a representative example of a host structure bearing the most common n -nodal set ($n = 6$) that features suitable cages to contain Cs⁺ ions.

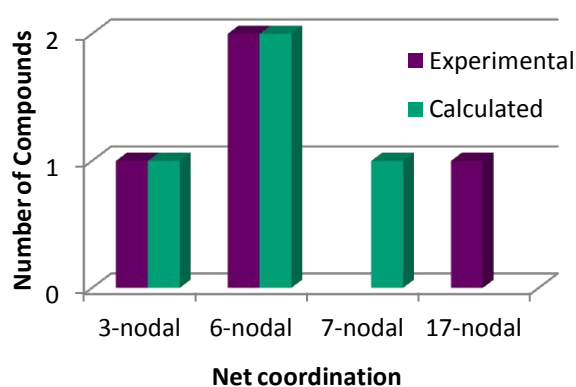
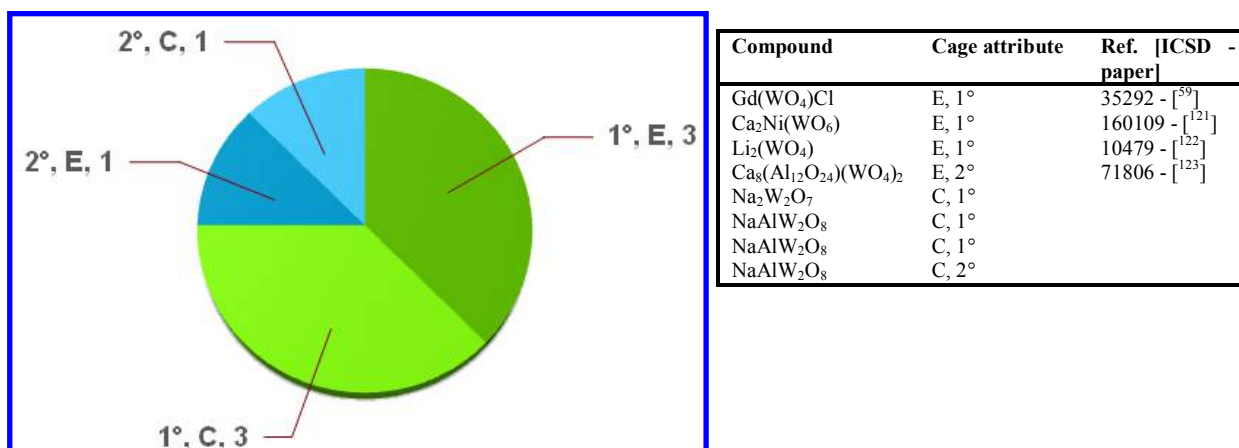
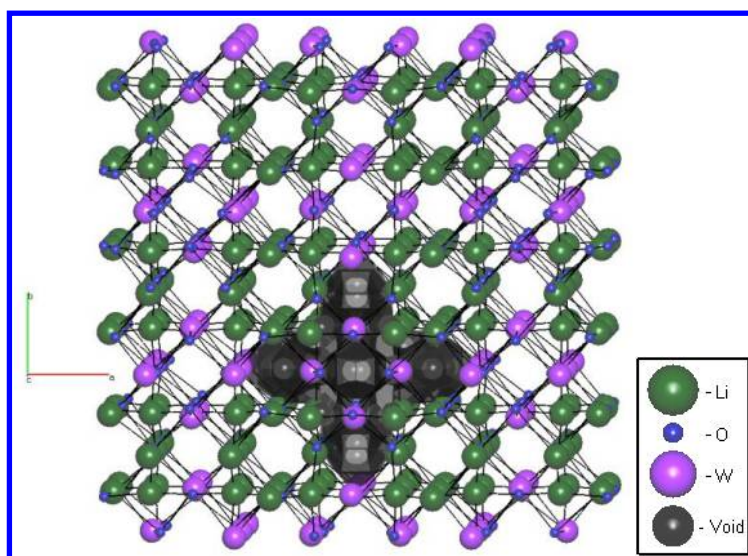


Figure 12. (left) Distribution of cage types (1°, 2°) of host structures comprising n-nodal nets that can incorporate Cs⁺ ions, according to their frequency observed in experimental (E) and calculated (C) crystal structures; (right) a list of their associated compound identifiers (ICSD number and reference citation).



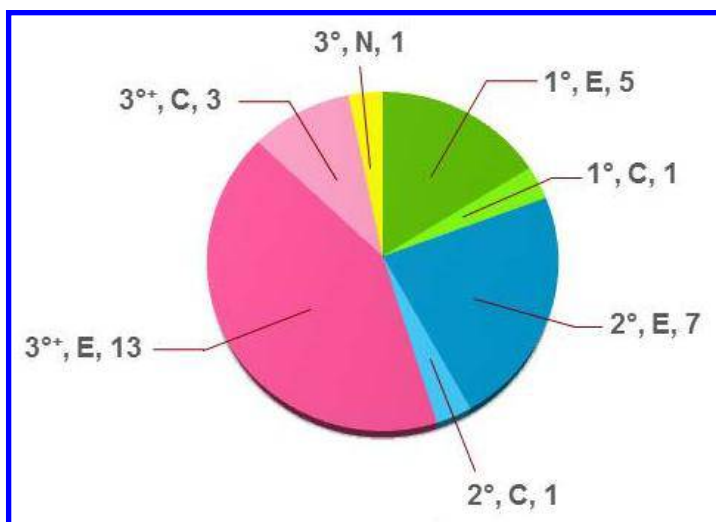


Figure 13. A representative example of a crystal structure (of $\text{Li}_2(\text{WO}_4)$ [ICSD ref. 10479 – [122]]) displaying the most common ($n = 6$) n-nodal net in which cages with suitable void space volumes (black/grey) reside to contain Cs^+ ions.

Sr^{2+} ions. The occupancy volume for Sr^{2+} ions (33.51 \AA^3), was obtained from the Slater empirical radius⁴⁴ in TOPOS. Void-space volume requirements for Sr^{2+} ions generated a targeted void space volume of $34 - 38 \text{ \AA}^3$. Within this range, the suitable cages of 20 previously reported structures bearing 24 cages ($5 \times 1^\circ$; $7 \times 2^\circ$; $13 \times 3^{\circ+}$; $3 \times$ multiple cages), five predicted ($1 \times 1^\circ$; $1 \times 2^\circ$; $3 \times 3^{\circ+}$), and one new crystal structure, ((2), bearing a 3° cage) were identified (Figure 14). A representative example structure that bears a 3-nodal net, the most common type of host framework whose cages appear suited to accommodate Sr^{2+} ions, is shown in Figure 15.

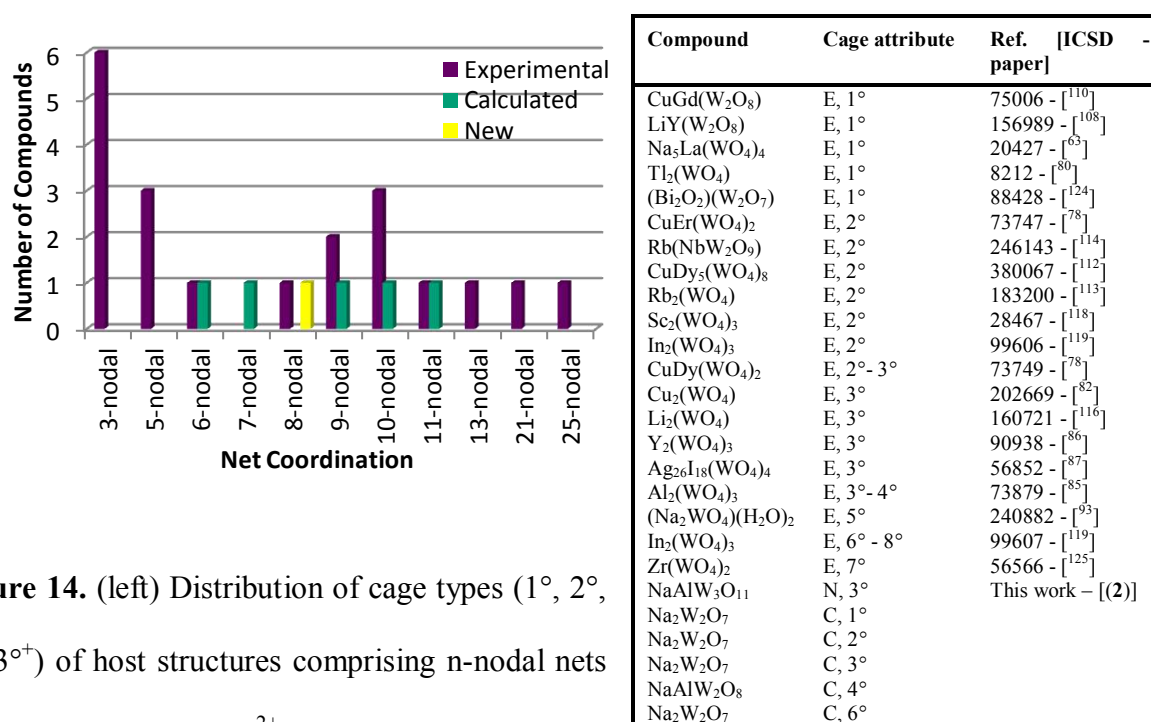


Figure 14. (left) Distribution of cage types (1°, 2°, 3°, 3⁺) of host structures comprising n-nodal nets that can incorporate Sr²⁺ ions, according to their frequency observed in previously reported (E) or newly-determined (N) experimental and calculated (C) crystal structures; (right) a list of their associated compound identifiers (ICSD number and reference citation).

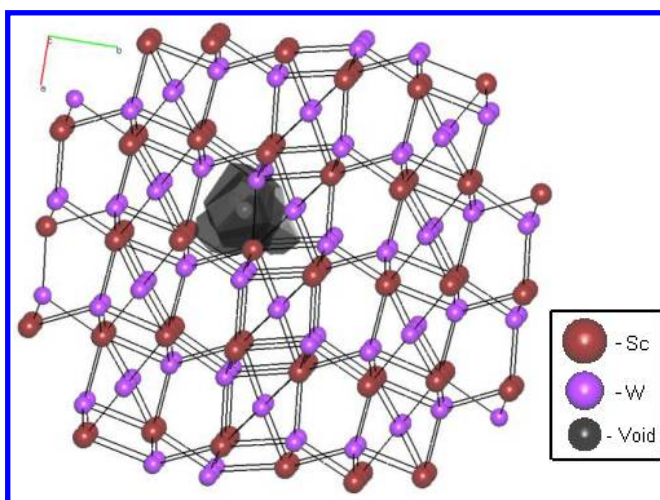
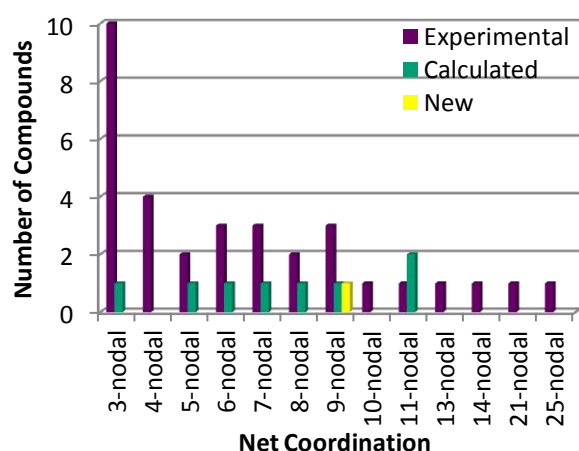
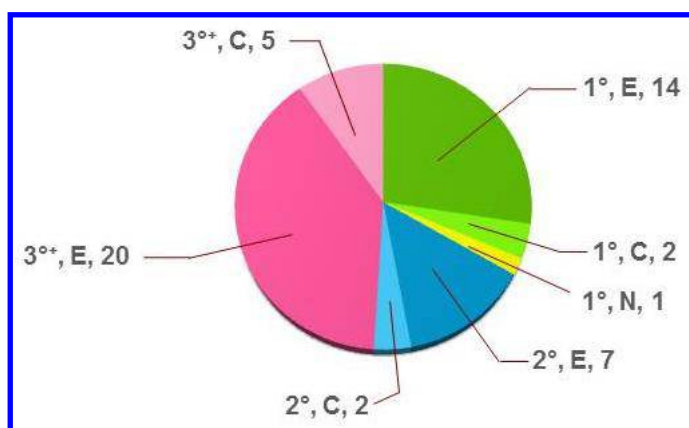


Figure 15. A representative example of a crystal structure (of $\text{Sc}_2(\text{WO}_4)_3$ [ICSD ref. 28467 – $[\text{118}]$]) manifesting the most common ($n = 3$) n-nodal net that contains cages with suitable void space volumes (black/grey) to accommodate Sr^{2+} ions.

Alternative Energy Storage.

CH_4 molecules. A target void-space volume of $29 - 33 \text{ \AA}^3$ for methane was obtained from a kinetic diameter of 3.8 \AA .⁴⁹ This resulted in the selection of 41 cages from 33 previously reported structures (14 x 1° ; 7 x 2° ; 20 x $3^{+\circ}$; 7 x multiple cages); 9 cages from 8 predicted structures (2 x 1° ; 2 x 2° ; 5 x $3^{+\circ}$; 1 x multiple cages), and a 1° cage in the newly-determined structure of (3). Figure 16 summarizes these trends. A representative example structure, bearing the most common type of n-nodal net ($n = 3$) whose cages appear to be able to host CH_4 molecules, is shown in Figure 17.



Compound	Cage attribute	Ref. [ICSD - paper]
CsLiWO ₄	E, 1°	14082 - [126]
RbGd(WO ₄) ₂	E, 1°	152962 - [127]
KBi(WO ₄) ₂	E, 1°	391361 - [128]
RbNd(WO ₄) ₂	E, 1°	155378 - [129]
K ₂ (UO ₂)(W ₂ O ₈)	E, 1°	96443 - [130]
Na ₅ Tb(WO ₄) ₄	E, 1°	20426 - [63]
Hg(WO ₄)	E, 1°	169667 - [65]
Li ₂ (UO ₂) ₄ (WO ₄) ₄ O	E, 1°	99481 - [131]
Li ₂ (WO ₄)	E, 1°	14196 - [132]
Y ₂ WO ₆	E, 1°	261479 - [133]
K ₂ (W(O ₂) ₄)	E, 1°	202672 - [134]
Na ₃ (W ₂ O ₇)	E, 1°	1883 - [32]
K ₂ W ₄ O ₁₃	E, 1°	2412 - [67]
Ca ₈ (Al ₁₂ O ₂₄)(WO ₄) ₂	E, 1°	62988 - [135]
U(WO ₄)	E, 2°	2285 - [115]
Cu ₂ WO ₄	E, 2°	62058 - [76]
Bi ₂ (WO ₆)	E, 2°	67647 - [136]
Al ₂ (WO ₄) ₃	E, 2°	73878 - [85]
La ₂ (WO ₄) ₃	E, 2°	78180 - [137]
Al ₂ (WO ₄) ₃	E, 2°	90936 - [86]
(Bi ₂ O ₂)(W ₂ O ₇)	E, 2° - 3°	88428 - [124]
CuEr(WO ₄) ₂	E, 3°	73747 - [78]
Rb ₄ H ₈ (H ₂ W ₁₂ O ₄₀)(H ₂ O) ₁₈	E, 3°	16468 - [138]
Li ₂ (WO ₄)	E, 3°	15395 - [117]
Al ₂ (WO ₄) ₃	E, 3°	56827 - [85]
Sc ₂ (WO ₄) ₃	E, 3° - 4°	28467 - [118]
In ₂ (WO ₄) ₃	E, 3° - 4°	99606 - [119]
Cu ₂ (WO ₄)	E, 4°	202669 - [82]
Y ₂ (WO ₄) ₃	E, 4° - 5°	90938 - [86]
Ag ₂₆ I ₁₈ (WO ₄) ₄	E, 5°	56852 - [87]
Al ₂ (WO ₄) ₃	E, 5° - 7°	73879 - [85]
(Na ₂ WO ₄)(H ₂ O) ₂	E, 6° - 7°	240882 - [93]
Zr(WO ₄) ₂	E, 8° - 9°	56566 - [125]
Na ₂ W ₂ O ₇	N, 1°	This work - [(3)]
Na ₂ WO ₄	C, 1°	
Na ₂ W ₂ O ₇	C, 1°	
NaAlW ₂ O ₈	C, 2°	
NaAlW ₂ O ₈	C, 2°	
Na ₂ W ₂ O ₇	C, 4°	
Na ₂ W ₂ O ₇	C, 5°	
NaAlW ₂ O ₈	C, 5° - 6°	
Na ₂ W ₂ O ₇	C, 7°	

Figure 16. (left) Distribution of cage types (1°, 2°, 3°) of host structures comprising n-nodal nets that can incorporate CH₄ molecules, according to their frequency observed in previously reported (E) or newly-determined (N) experimental and calculated (C) crystal structures; (right) a list of their associated compound identifiers (ICSD number and reference citation).

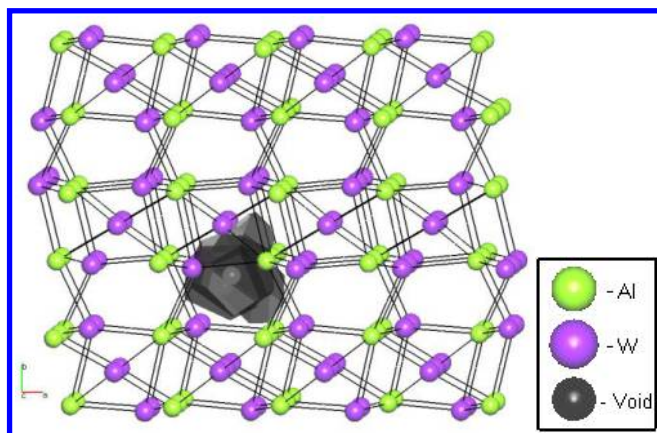
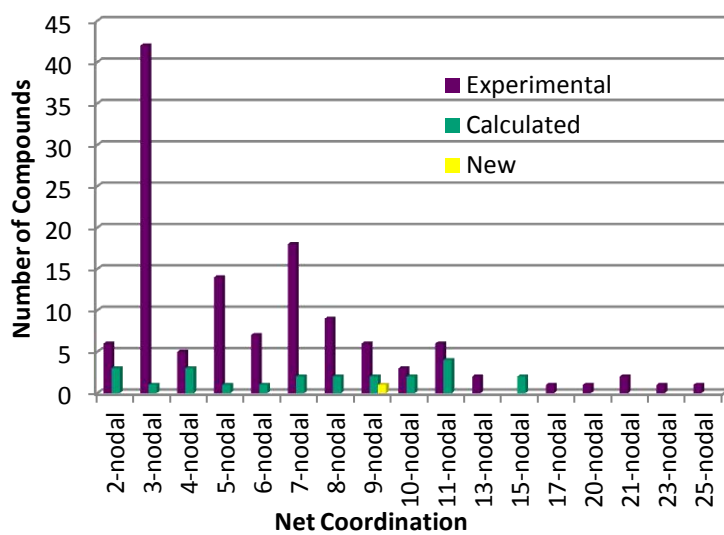
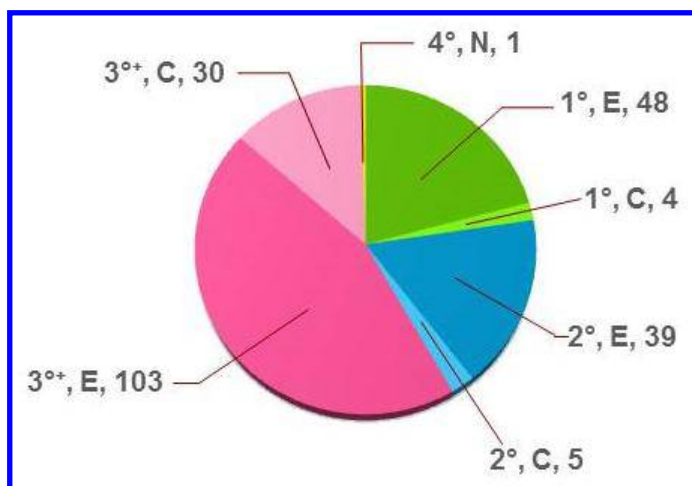


Figure 17. A representative example of a crystal structure (of $\text{Al}_2(\text{WO}_4)_3$ [ICSD ref. 90936 – [86]]) illustrating the most common n-nodal ($n = 3$) net in which cages with suitable void space volumes (black/grey) can host CH_4 molecules.

H_2 molecules. The target volume of H_2 was determined using a kinetic diameter of 2.89 \AA ,¹⁹ resulting in a target void-space volume range of $13 - 17 \text{ \AA}^3$. 190 suitable cages to host H_2 were found in 124 previously reported structures (48 x 1° ; 39 x 2° ; 103 x 3^{0+} ; 39 x multiple cages); 39 cages in 23 predicted structures (4 x 1° ; 5 x 2° ; 30 x 3^{0+} ; 11 x multiple cages); and the in-house determined crystal structure, **(3)** (4°); as seen in Figure 18. Interestingly, eight of the previously reported, as well as one of the predicted structures, each contain at least four suitable types of cages for hosting H_2 . Figure 19 displays a representative example of a tungstate-based framework structure bearing the most common n-nodal set ($n = 3$) with suitable cages to host H_2 molecules.



Compound	Cage attribute	Ref. [ICSD -paper]
Li(NbWO ₆)	E, 1°	202779 - [139]
Li(NbWO ₆)	E, 1°	202780 - [139]
K((SbW)O ₆)	E, 1°	181570 - [140]
Cs(SbWO ₆)	E, 1°	165063 - [141]
KNb(WO ₆)	E, 1°	63562 - [142]
AgIn(WO ₄) ₂	E, 1°	60373 - [143]
LiLaW ₂ O ₈	E, 1°	261829 - [144]
LiGdW ₂ O ₈	E, 1°	261833 - [144]
LiSmW ₂ O ₈	E, 1°	261831 - [144]
LiEuW ₂ O ₈	E, 1°	261832 - [144]
LiNdW ₂ O ₈	E, 1°	261830 - [144]
Cs(TaWO ₆)	E, 1°	165061 - [141]
NaBi(WO ₄) ₂	E, 1°	168136 - [145]
Pb ₂ Co(WO ₆)	E, 1°	77912 - [146]
Sr ₂ Zn(WO ₆)	E, 1°	72811 - [147]
Sr ₂ Mg(WO ₆)	E, 1°	152575 - [148]
Ba ₂ (CoWO ₆)	E, 1°	97029 - [149]
Ba ₂ CoWO ₆	E, 1°	27425 - [150]
Ba ₂ NiWO ₆	E, 1°	27426 - [150]
Ba ₂ (FeWO ₆)	E, 1°	95520 - [151]
Pb ₂ Mg(WO ₆)	E, 1°	67880 - [152]
Ba ₂ ZnWO ₆	E, 1°	423034 - [153]
Ba ₂ Ca(WO ₆)	E, 1°	245599 - [154]
NaIn(WO ₄) ₂	E, 1°	16263 - [155]
Ni(WO ₄)	E, 1°	16685 - [156]
CrWO ₄	E, 1°	36213 - [157]
Ca(WO ₄)	E, 1°	155424 - [158]
Ca(WO ₄)	E, 1°	155423 - [158]
NaIn(WO ₄) ₂	E, 1°	28098 - [159]
Sr(WO ₄)	E, 1°	155425 - [158]
Pb(WO ₄)	E, 1°	155522 - [160]
Ba(WO ₄)	E, 1°	155513 - [160]
Pb ₂ Co(WO ₆)	E, 1°	72905 - [161]
Ba ₂ MgWO ₆	E, 1°	423033 - [153]
Na ₂ (WO ₄)	E, 1°	44524 - [162]
Hg(WO ₄)	E, 1°	169671 - [65]
Nd(WO ₃ N)	E, 1° - 2°	99740 - [163]
NaDy(WO ₄) ₂	E, 1° - 2°	248012 - [164]
NaBi(WO ₄) ₂	E, 1° - 2°	83318 - [165]
NaNd(WO ₄) ₂	E, 1° - 2°	66091 - [166]
NaGd(WO ₄) ₂	E, 1° - 2°	157390 - [167]
NaLa(WO ₄) ₂	E, 1° - 2°	66090 - [166]
Pb(WO ₄)	E, 1° - 2°	75981 - [168]
(LiLa)(WO ₄) ₂	E, 1° - 2°	184015 - [169]
Sr(WO ₄)	E, 1° - 3°	155426 - [158]
Pb(WO ₄)	E, 1° - 3°	155518 - [160]
Na ₂ ZrW ₃ O ₁₂	E, 1° - 3°	20405 - [170]
Eu ₃ (BWO ₉)	E, 1° - 4°	39810 - [171]
KLu(WO ₄) ₂	E, 2°	95541 - [172]
CsLu(WO ₄) ₂	E, 2°	202270 - [173]
KEu(WO ₄) ₂	E, 2°	173634 - [53]
KLu(WO ₄) ₂	E, 2°	172510 - [95]
KYb(WO ₄) ₂	E, 2°	280877 - [96]
KEr(WO ₄) ₂	E, 2°	157832 - [97]
KY(WO ₄) ₂	E, 2°	411285 - [98]
KHo(WO ₄) ₂	E, 2°	182626 - [99]
Ba(TeW ₂ O ₉)	E, 2°	281502 - [174]
La ₃ (BWO ₉)	E, 2°	39809 - [171]
Eu ₃ (BWO ₉)	E, 2°	150338 - [175]
Dy ₃ (BWO ₉)	E, 2°	250419 - [55]
Tb ₃ (BWO ₉)	E, 2°	250418 - [55]
Gd ₃ (BWO ₉)	E, 2°	250417 - [55]
Nd ₃ (BWO ₉)	E, 2°	250415 - [55]
Sm ₃ (BWO ₉)	E, 2°	250416 - [55]
Pr ₃ (BWO ₉)	E, 2°	250414 - [55]
KBi(WO ₄) ₂	E, 2°	391361 - [128]
La ₂ (WO ₄)(Te ₃ O ₇) ₂	E, 2°	249538 - [58]
Ba ₁₁ (W ₄ O ₂₃)	E, 2°	418207 - [36]
Y ₂ WO ₆	E, 2°	261479 - [133]
K ₂ (TeW ₃ O ₁₂)	E, 2°	97506 - [176]
Rb ₂ (W ₂ O ₇)	E, 2°	300230 - [177]
Hg(WO ₄)	E, 2°	169667 - [65]
LiW ₃ O ₉	E, 2° - 3°	38310 - [178]
Li ₂ (UO ₂)(WO ₄) ₂	E, 2° - 3°	99480 - [131]

Compound	Cage attribute	Ref. [ICSD - paper]
NdNa ₅ (WO ₄) ₄	E, 2° - 4°	6145 - [179]
BiLaWO ₆	E, 3°	416793 - [52]
BiNdWO ₆	E, 3°	416789 - [52]
Pr ₃ (WO ₆)Cl ₃	E, 3°	20626 - [105]
La ₃ WO ₆ Cl ₃	E, 3°	35595 - [106]
LiY(W ₂ O ₈)	E, 3°	156989 - [108]
KNd(WO ₄) ₂	E, 3°	9364 - [180]
Ca ₃ WO ₅ Cl ₂	E, 3°	2335 - [181]
Li ₂ (UO ₂) ₄ (WO ₄) ₄ O	E, 3°	99481 - [131]
Nd(WO ₄)(OH)	E, 3°	27731 - [182]
Pb ₂ B ₂ WO ₁₂	E, 3°	261534 - [183]
Rb ₂ (TeW ₃ O ₁₂)	E, 3°	97507 - [176]
K ₂ (UO ₂)(W ₂ O ₈)	E, 3° - 5°	96443 - [130]
Li ₂ Cu(WO ₄) ₂	E, 3° - 5°	92854 - [101]
Na ₄ Th(WO ₄) ₄	E, 3° - 5°	422185 - [61]
Li ₂ Ni(WO ₄) ₂	E, 3° - 5°	92853 - [101]
Li ₂ Co(WO ₄) ₂	E, 3° - 6°	92852 - [101]
Na ₃ W ₂ O ₇ (H ₂ O)	E, 3° - 6°	408189 - [184]
Na ₃ F(WO ₄)	E, 4°	417289 - [73]
Rb ₄ H ₈ (H ₂ W ₁₂ O ₄₀)(H ₂ O) ₁₈	E, 4°	164668 - [138]
Na ₂ (W ₂ O ₇)	E, 4°	1883 - [32]
K ₂ W ₄ O ₁₃	E, 4°	2412 - [67]
Ca ₈ (Al ₁₂ O ₂₄)(WO ₄) ₂	E, 4°	71806 - [123]
UW ₃ O ₁₁	E, 4°	81983 - [75]
ErBi(W ₂ O ₆)	E, 4° - 5°	183443 - [72]
EuBi(W ₂ O ₆)	E, 4° - 5°	183444 - [72]
Rb ₂ (WO ₄)	E, 4° - 5°	183200 - [113]
Li ₂ (W ₂ O ₇)	E, 4° - 5°	1897 - [71]
SmBi(W ₂ O ₆)	E, 4° - 5°	183445 - [72]
Bi ₂ WO ₆	E, 4° - 6°	171328 - [102]
Na ₅ Lu(WO ₄) ₄	E, 4° - 7°	200930 - [62]
Na ₅ Tb(WO ₄) ₄	E, 4° - 7°	20426 - [63]
Rb ₁₂ (Nb ₃₀ W ₃ O ₉₀)	E, 5°	1505 - [107]
CuGd(W ₂ O ₈)	E, 5° - 6°	75006 - [110]
LiPr(WO ₄) ₂	E, 5° - 6°	200520 - [111]
Na ₅ Y(WO ₄) ₄	E, 5° - 9°	417143 - [74]
Na ₅ La(WO ₄) ₄	E, 5° - 9°	20427 - [63]
CuDy(WO ₄) ₂	E, 6°	73749 - [78]
CuEr(WO ₄) ₂	E, 6°	73747 - [78]
CuSm(W ₂ O ₈)	E, 6°	68615 - [79]
CuLa(W ₂ O ₈)	E, 6° - 7°	68614 - [79]
Al ₂ (WO ₄) ₃	E, 7°	73878 - [85]
Al ₃ (WO ₄) ₃	E, 7°	90936 - [86]
Sc ₂ (WO ₄) ₃	E, 7°	28467 - [118]
U(WO ₄)	E, 7° - 8°	2285 - [115]
K ₂ Nb ₁₀ W ₇ O ₄₇	E, 7° - 8°	62130 - [84]
Cu ₂ (WO ₄)	E, 7° - 10°	202669 - [82]
Ce ₁₀ W ₂ O ₈₁	E, 8° - 10°	260095 - [81]
Ag ₂₆ I ₁₈ (WO ₄) ₄	E, 9°	56852 - [87]
FeCe(WO ₄)(W ₂ O ₈)	E, 9° - 10°	401919 - [83]
Na ₂ W ₂ O ₇	N, 4°	This work - [(3)]
NaAlW ₂ O ₈	C, 1°	
NaAlW ₂ O ₈	C, 1° - 2°	
NaAlW ₂ O ₈	C, 1° - 2°	
NaAlW ₂ O ₈	C, 1° - 2°	
Na ₂ WO ₄	C, 2°	
Na ₂ W ₂ O ₇	C, 2° - 3°	
Na ₂ WO ₄	C, 3°	
Na ₂ WO ₄	C, 3°	
Na ₂ W ₂ O ₇	C, 3°	
Na ₄ WO ₅	C, 3° - 4°	
Na ₂ W ₂ O ₇	C, 4°	
Na ₂ W ₄ O ₁₃	C, 4°	
NaAlW ₂ O ₈	C, 4°	
Na ₂ W ₂ O ₇	C, 5°	
Na ₂ WO ₄	C, 5° - 6°	
NaAlW ₂ O ₈	C, 5° - 6°	
NaAlW ₂ O ₈	C, 5° - 7°	
Na ₂ W ₂ O ₇	C, 5° - 9°	
Na ₂ W ₄ O ₁₃	C, 6°	
NaAlW ₂ O ₈	C, 6°	
NaAlWO ₅	C, 6° - 7°	

NaAlW ₂ O ₈	C, 6° - 8°
Na ₂ W ₂ O ₇	C, 10°

Figure 18. (top) Distribution of cage types (1°, 2°, 3⁺, 4°) of host structures comprising n-nodal nets that can incorporate H₂ molecules, according to their frequency observed in previously reported (E) or newly-determined (N) experimental and calculated (C) crystal structures; (bottom) a list of their associated compound identifiers (ICSD number and reference citation).

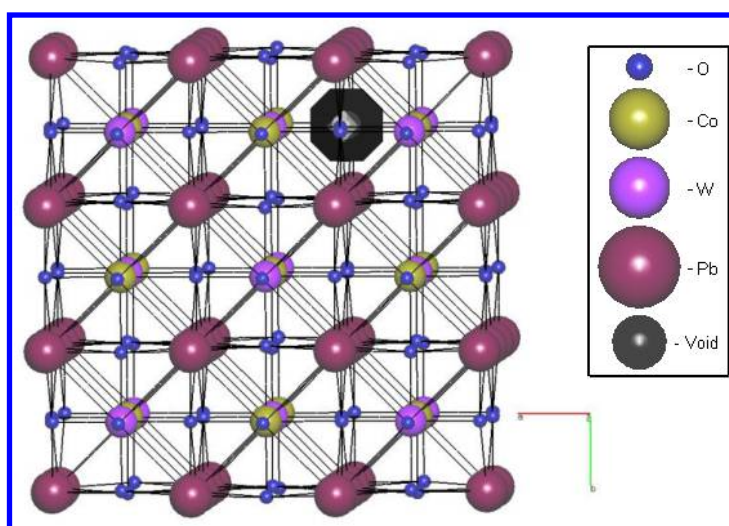


Figure 19. A representative example of a crystal structure (of Pb₂Co(WO₆) [ICSD ref. 72905 – [161]]) displaying the most common n-nodal (n = 3) net in which cages with suitable void space volumes (black/grey) can host H₂ molecules.

General trends

Topological patterns and frequency trends in guest-host matching preferences. One of the main objectives of this study was the discovery of potential trends in topological patterns of tungstate framework structures with respect to their desired guest type. The results of the

1
2
3 experimentally-determined structures clearly demonstrate that for smaller (H_2 , U or Pu) and
4
5 medium-sized (CH_4 , or Sr^{2+}) guests, compounds with 3-nodal nets are the most abundant. In
6
7 this context, the small guest molecule CO_2 is an exception since it prefers 5- and 6-nodal
8
9 structures. Within each of the predominant net classifications, the majority of the best suited
10
11 cages for guests were found to be 3° , aside from those involving the two smallest guest types.
12
13 Here, CO_2 is best hosted almost exclusively in 1° , 2° , or 3° cages of 5- or 6-nodal nets,
14
15 whereas H_2 finds suitable host accommodation predominantly in the 1° cages of 3-nodal nets.
16
17 It transpires that the three largest guests, PuO_2 , UO_2 , and Cs^+ , prefer higher-nodal nets, and
18
19 they can be hosted exclusively in 1° cages within their preferred n-nodal nets.
20
21
22
23
24

25
26 In contrast, computationally-derived structures indicate that tungstate frameworks with
27
28 higher-order nodal nets are preferred hosts, and several guest types (CO_2 , H_2 , CH_4) showed
29
30 promise for their inclusion into 11-nodal net structures. The preferred hosts for U and Pu
31
32 ions were 4-nodal nets, whereas Cs^+ preferred 6-nodal nets. For PuO_2 , and UO_2 only one
33
34 calculated structure, featuring an 8-nodal, and a 10-nodal net, respectively, was deemed a
35
36 suitable host, while Sr^{2+} guests did not exhibit any dominant net-type for their host structures.
37
38
39
40

41 **Experimentally-derived versus hypothetical tungstates structures: trends and biases.**

42
43 This discrepancy in host-guest matching preferences between predicted- and experimentally-
44
45 determined structures may arise from a variety of factors. Firstly, this is a rather complicated
46
47 comparison, given that the computationally-determined hypothetical structures exclusively
48
49 considered possible variations of $Na_aAl_bW_cO_d$ (where a, c, d may be any integer and b may
50
51 be any integer or zero), whereas the generated set of experimentally-determined structures
52
53 was far less restrictive: including any structure that contains W, O, and one or two other
54
55 elements. The host-guest matching preferences determined using the computationally-
56
57 derived structural set might naturally be refined if hypothetical tungstate structures were
58
59
60

1
2
3 generated for all of the possible chemical compositions that are accepted in the
4 experimentally-derived structural set; although such a quest would be computationally
5 expensive and laborious. So turning this problem on its head, if all compounds with the
6 general formula $\text{Na}_a\text{X}_b\text{W}_c\text{O}_d$ (where X is any element) are isolated from the experimentally-
7 derived structural data set, a preference trend towards nets of higher order - mostly 5-, 8-, and
8 9-nodal nets - can be observed, *i.e.* experimental and computational results apparently tend
9 towards a common preference of higher-order nodal nets as suitable hosts. However, with
10 one exception, these trends have to be considered with caution, owing to the very limited
11 numbers of compounds available for each guest type as a result of this data restriction. The
12 exception concerns the set of possible hosts for H_2 ; in this case, 3-nodal nets remained
13 preferred for both the full experimental findings and within this experimental source
14 restriction to $\text{Na}_a\text{X}_b\text{W}_c\text{O}_d$.

15
16
17 Secondly, this host-guest matching preference discrepancy may be due to the generated cage
18 volumes in the theoretically-calculated structures, which were typically larger than those
19 encountered in experimentally determined structures. Nonetheless, observed differences are
20 cage size and type dependent. For example, primary cages for the largest cage sizes compare
21 well between hypothetically and experimentally generated structures (329.35 \AA^3 and 326.95
22 \AA^3 , respectively, on average). Discord appears more at the detailed level and this reflects
23 more of a classification problem than a straight-forward difference between theory and
24 experiment. This can be illustrated by a consideration of some primary cage statistics. If these
25 primary cage sizes are separated into volumes ranges, and a percentage is constructed for the
26 number of primary cages found in each volume range versus the total number of primary
27 cages, differences become more apparent. In this respect, experimental structures have 8% of
28 primary cages in the $>100 \text{\AA}^3$ range, 16% within 50-100 \AA^3 , 31% within 20-50 \AA^3 , and 45%
29
30
31
32
33
34
35
36
37
38
39
40
41
42
43
44
45
46
47
48
49
50
51
52
53
54
55
56
57
58
59
60

1
2
3 20 \AA^3. In contrast, calculated structures have 35% of primary cages in the >100 \AA^3 range,
4
5 23% within 50-100 \AA^3 , 33% within 20-50 \AA^3 , and 9% 20 \AA^3. In addition, a greater number
6
7 of distinct cages were found in many cases for the theoretically calculated structures. Again,
8
9 some statistics are helpful for explanation: 62.3% of experimental structures possess 1-10
10
11 total cages, 24.3% have 11-20 total cages, 8.1% have 21-30 total cages, 4.2% have 31-40
12
13 total cages, 0.7% have 41-50 total cages, and 0.4% have >50 total cages. In contrast, 18.6%
14
15 of calculated structures have 1-10 total cages, 39.5% have 11-20 total cages, 14.0% have 21-
16
17 30 total cages, 9.3% have 31-40 total cages, 2.3% have 41-50 total cages, and 16.3% have
18
19 >50 total cages. Furthermore, despite comprising a higher absolute number of cages, often
20
21 fewer cages of distinct volumes were found for the calculated relative to the experimental
22
23 structures owing to many cages numerically producing the same volume as other cages
24
25 within a single structure.
26
27
28
29
30
31

32
33 Thirdly, databases of experimentally-determined crystal structures contain an intrinsic
34
35 chemical bias since the determination of a crystal structure is predicated on a systematic
36
37 distortion of chemical space, on several accounts. For example, some classes of chemicals
38
39 are easier to crystallize than others, and obtaining crystals of a compound naturally facilitates
40
41 its likelihood of associated crystal structure determination. Certain families of compounds
42
43 will also appear in a crystal structure database with greater frequency than others, or even
44
45 exist in duplicate or manifold. Possible causes of this include synthetic efforts being prolific
46
47 in a specific area of chemistry where compounds are in vogue for a popular application; or
48
49 the prevalence of polymorphism in a series of chemicals that issues duplicate chemical
50
51 structures that bear different space groups.
52
53
54
55

56
57 In the context of the subject study, this chemical bias could manifest as clusters of preferred
58
59 nets owing to the large grouping of chemical families with similar structures. Indeed, such
60

1
2
3 clustering is borne out in this study. One example of it features in the list of ‘ideal net’
4
5 compounds that could host H₂, which includes five compounds with the formula LiXW₂O₈
6
7 (X = lanthanide). These families of compounds will naturally form similar nets, as their
8
9 chemical connectivity is similar. Another example concerns the possible hosts for CH₄,
10
11 amongst which four different space groups of Al₂(WO₄)₃ can be found: Pbcn, Pnca, P2₁/n,
12
13 and P2₁, i.e. the replication of chemical formula but distinguished by polymorphism. Again,
14
15 all of these result in the same, or similar, nets.
16
17
18
19

20
21 While computationally-derived structural data sets also have the ability to feature chemical
22
23 bias, such bias would have to be generated by the user, and good practice in computational
24
25 research is usually able to circumvent any significant biases at the level of those present in
26
27 large sets of experimental data. This experimental bias therefore augments the level of
28
29 discrepancy between experimental and computationally derived host-guest matching
30
31 preferences.
32
33
34
35

36
37 **How do the in-house determined crystal structures (1)-(3) rate as potential hosts and**
38
39 **present within the broader set of tungstate structural frameworks?** The in-house
40
41 determined crystal structure of (1) contained only two cages: one relatively large (66.03 Å³),
42
43 and a relatively small one (5.28 Å³). These cages were only able to accommodate one of the
44
45 guest types (UO₂) explored in this study. The crystal structure of (1) represents the first
46
47 report of its structural type for the formula, NaAlW₂O₈. Hypothetical structures that
48
49 conformed to the same formula, but exhibited different frameworks, were nonetheless
50
51 identified; and when taken collectively, they were predicted to be able to accommodate all
52
53 but two guest types (PuO₂, and UO₂).
54
55
56
57
58
59
60

1
2
3 Void-space analysis indicates that the crystal structure of **(2)** can accommodate PuO_2 , UO_2 ,
4 or Sr^{2+} . The rarity of this crystal structure is even more stark than that of **(1)**, being the first
5 report of any structural type with formula, $\text{NaAlW}_3\text{O}_{11}$. The fact that not even any
6 hypothetical structures of this formula were predicted via the computational aspect of this
7 study is particularly interesting. As noted earlier, the fundamental strategy behind the
8 structure prediction method used herein is based on the statistical likelihood of ionic
9 substitution of previously reported crystal structures. The lack of any hypothetical structures
10 of this formula in its prediction set is therefore symptomatic of no other previously reported
11 experimental structures of this formula well beyond just tungstates. It would thus seem that
12 the crystal structure of **(2)** is rare indeed, to the extent that it could now be used as an
13 exemplar to help ionic substitution methods start to predict isomorphous structures of other
14 (non-tungstate) inorganic frameworks. The structure determination of **(2)** was in fact
15 particularly challenging, and so the use of this first structural exemplar in concert with this
16 type of structural prediction method could go one step further, by offering computation the
17 possibility to help guide the experimental crystallographer to probable solutions of
18 isomorphous structures. An example of such a concerted approach, whose premise is built
19 upon similar lines, is that of Meredig and Wolverton.¹⁸⁵

20
21
22 Among the three in-house determined crystal structures, **(3)** offers the most options for
23 hosting the guests explored in this study, being able to accommodate U or Pu ions as well as
24 CH_4 and H_2 molecules. In addition, the corresponding hypothetical structures of $\text{Na}_2\text{W}_2\text{O}_7$
25 were able to host all guests, except for PuO_2 , in at least one manifestation of this chemical
26 formula. It is worth remembering that the room-temperature crystal structure of **(3)** has been
27 reported previously, so statistical inferences behind the structure prediction method used in
28 this study are facilitated with pre-existing crystal structure evidence. The fact that **(3)** differs
29
30
31
32
33
34
35
36
37
38
39
40
41
42
43
44
45
46
47
48
49
50
51
52
53
54
55
56
57
58
59
60

1
2
3 from (1) and (2) by its chemical lack of Al is presumably also significant to the nature of
4 these host-guest matching preferences. In any event, the finding that (3) offers the most
5 abundant selection of host-guest matching preferences amongst our three in-house available
6 materials, means that we now have a practical guide forward for prioritizing experimental
7 host-guest adsorption studies on these compounds.
8
9
10
11
12
13
14
15
16

17 **Concluding remarks and future outlook**

18
19
20 Void space analysis of 577 tungstate crystal structures, mined from experimentally- and
21 computationally-derived data sources, offers an important first step towards identifying new
22 host materials for environmentally important small molecules and ions. 196 hypothetical
23 tungstate structures were generated using the recently developed structure prediction methods
24 that exploit the statistical likelihood of ionic substitution;³⁸ 378 experimentally determined
25 crystal structures of tungstates were sourced from the ICSD and coupled with three in-house
26 crystal structure determinations of tungstate materials, (1)-(3). It transpired that NaAlW₂O₈
27 (1) and NaAlW₃O₁₁ (2) present somewhat rare crystal structures; and while (2) appears well
28 suited to host several nuclear waste materials, Na₂W₂O₇ (3) is predisposed to accommodate
29 small molecules, CH₄ and H₂, for alternative energy applications, as well as industrially
30 relevant ions for containing nuclear waste.
31
32
33
34
35
36
37
38
39
40
41
42
43
44
45
46
47

48 Beyond the immediate practical considerations of these three in-house available materials, the
49 data-mining aspect of this study pinpoints a number of other tungstate framework structures
50 that can, when taken collectively, host the entire range of environmentally important
51 molecules and ions explored in this study (CO₂, UO₂, PuO₂, U, Pu, Cs⁺, Sr²⁺, CH₄, and H₂).
52 To this end, these results offer good prospects for tungstate compounds as viable host
53 materials for environmental storage applications. Some of these other tungstate structures
54
55
56
57
58
59
60

1
2
3 may even host certain guests better than the in-house tungstate materials immediately
4 available to us. However, the scope of this study essentially provides a binary outcome for a
5 given framework structure: either the structure is, or is not, able to host a given guest. While
6 this study illustrates a preference to certain types of n-nodal structures by virtue of their
7 observed frequency, this does not imply directly that these preferred hosts are superior to
8 those less commonly found. There are currently no formal ranking criteria that define one
9 tungstate compound over another as being better able to host a given type of guest. It would
10 be natural to develop such a ranking formalism as these void-space analysis methods
11 continue to evolve. To this end, comparison with other host/guest prediction methods, such as
12 channel evaluation,²⁶ or substructural similarity functions¹⁸⁶ might prove useful. This will
13 further assist the experimentally-minded materials scientist in selecting their host material to
14 most optimally store small, but environmentally important, molecules or ions.

15
16
17
18
19
20
21
22
23
24
25
26
27
28
29
30
31
32
33 Notwithstanding the powerful practical bearing of generating a catalogue of material
34 selections that could ultimately allow one to simply ‘dial up’ a request to match a host
35 structure to a desired guest, it should also be remembered that the currently predicted host
36 frameworks have hypothetical as well as experimental crystal structure origins, so some of
37 these tungstate materials have yet to be experimentally realized; the combined sets of
38 experimentally and computationally generated data are also currently limited. In the spirit of
39 considering further developments of this approach, a more explicit parameterization of guest
40 shape may also help to refine the host-guest matching preferences predicted by this study.

41
42
43
44
45
46
47
48
49
50
51
52
53 Looking ahead, it should be remembered that this study has only shown how to physically fit
54 guest types into cages of host structures; it has not considered the fabrication method of the
55 host-guest composite. Indeed, this is a study in its own right, and much research has been
56 engaged with studying the dynamic processes associated with adsorption of a specific guest

1
2
3 into an individual host;^{187,188} or nanofabrication routes that render *in situ* host-guest synthesis
4
5 where the guest is embedded into the host in a concerted fashion.^{189,190} The subject study
6
7 represents more of a ‘ship in a bottle’ perspective, considering the final outcome, pending the
8
9 experimental adsorption conditions (heat, pressure, reaction phase, etc) or concerted host-
10
11 guest nanofabrication methods can be resolved. Ideally, this ‘ship in a bottle’ approach,
12
13 which surveys a broad set of structures, will ultimately go hand-in-hand with simulations of
14
15 adsorption dynamics or nanofabrication of individual guest-host composites, that can be
16
17 short-listed via our procedure; with auxiliary considerations that ensure chemical
18
19 compatibility between host and guest. Creating such a unified effort will enable an ‘all-in-
20
21 one’ prediction of molecular storage capabilities and its associated synthetic processing.
22
23
24
25
26
27

28 **Acknowledgements**

29
30
31 Velin Nikolov from the Bulgarian Academy of Sciences is gratefully acknowledged for
32
33 supplying the samples of tungstate materials (1)-(3). John J. Rickard from the Cavendish
34
35 Laboratory, University of Cambridge, is thanked for his technical assistance with the EDX
36
37 experiment. J. M. C. is indebted to the Fulbright Commission for a UK-US Fulbright Scholar
38
39 Award hosted by Argonne National Laboratory where work done was supported by DOE
40
41 Office of Science, Office of Basic Energy Sciences, under Contract No. DE-AC02-
42
43 06CH11357.
44
45
46
47

48
49 **Supplementary Information** Crystallographic information files for (1)-(3) are provided as
50
51 Supplementary Information and are available from the corresponding author.
52

53 **References**

- 54
55
56
57 (1) Pires, J.; Carvalho, A.; de Carvalho, M. B. Adsorption of Volatile Organic Compounds
58
59 in Y Zeolites and Pillared Clays. *Microporous Mesoporous Mater.* **2001**, *43* (3), 277–
60
287.

- 1
2
3 (2) Shu, H.-T.; Li, D.; Scala, A. A.; Ma, Y. H. Adsorption of Small Organic Pollutants
4 from Aqueous Streams by Aluminosilicate-Based Microporous Materials. *Sep. Purif.*
5 *Technol.* **1997**, *11* (1), 27–36.
6
7
- 8 (3) Millward, A. R.; Yaghi, O. M. Metal-Organic Frameworks with Exceptionally High
9 Capacity for Storage of Carbon Dioxide at Room Temperature. *J. Am. Chem. Soc.*
10 **2005**, *127* (51), 17998–17999.
11
12
- 13 (4) Drabarek, E.; McLeod, T. I.; Hanna, J. V.; Griffith, C. S.; Luca, V. Tungstate-Based
14 Glass–ceramics for the Immobilization of Radio Cesium. *J. Nucl. Mater.* **2009**, *384*
15 (2), 119–129.
16
17
- 18 (5) Luca, V.; Griffith, C. S.; Drabarek, E.; Chronis, H. Tungsten Bronze-Based Nuclear
19 Waste Form Ceramics. Part 1. Conversion of Microporous Tungstates to Leach
20 Resistant Ceramics. *J. Nucl. Mater.* **2006**, *358* (2-3), 139–150.
21
22
- 23 (6) Luca, V.; Drabarek, E.; Chronis, H.; McLeod, T. Tungsten Bronze-Based Nuclear
24 Waste Form Ceramics. Part 3: The System Cs_{0.3}MxW_{1-x}O₃ for the Immobilization
25 of Radio Cesium. *J. Nucl. Mater.* **2006**, *358* (2-3), 164–175.
26
27
- 28 (7) Griffith, C. S.; Sebesta, F.; Hanna, J. V.; Yee, P.; Drabarek, E.; Smith, M. E.; Luca, V.
29 Tungsten Bronze-Based Nuclear Waste Form Ceramics. Part 2: Conversion of
30 Granular Microporous Tungstate–polyacrylonitrile (PAN) Composite Adsorbents to
31 Leach Resistant Ceramics. *J. Nucl. Mater.* **2006**, *358* (2-3), 151–163.
32
33
- 34 (8) Eddaoudi, M.; Kim, J.; Rosi, N.; Vodak, D.; Wachter, J.; O’Keeffe, M.; Yaghi, O. M.
35 Systematic Design of Pore Size and Functionality in Isoreticular MOFs and Their
36 Application in Methane Storage. *Science* **2002**, *295* (5554), 469–472.
37
38
- 39 (9) Msayib, K. J.; Book, D.; Budd, P. M.; Chaukura, N.; Harris, K. D. M.; Helliwell, M.;
40 Tedds, S.; Walton, A.; Warren, J. E.; Xu, M.; et al. Nitrogen and Hydrogen Adsorption
41 by an Organic Microporous Crystal. *Angew. Chemie* **2009**, *121* (18), 3323–3327.
42
43
- 44 (10) Furukawa, H.; Yaghi, O. M. Storage of Hydrogen, Methane, and Carbon Dioxide in
45 Highly Porous Covalent Organic Frameworks for Clean Energy Applications. *J. Am.*
46 *Chem. Soc.* **2009**, *131* (25), 8875–8883.
47
48
- 49 (11) Chun, H.; Moon, J. Discovery, Synthesis, and Characterization of an Isomeric
50 Coordination Polymer with Pillared Kagome Net Topology. *Inorg. Chem.* **2007**, *46*
51 (11), 4371–4373.
52
53
- 54 (12) Li, H.; Eddaoudi, M.; O’Keeffe, M.; Yaghi, O. M. Design and Synthesis of an
55 Exceptionally Stable and Highly Porous Metal-Organic Framework. *Nature* **1999**, *402*
56 (6759), 276–279.
57
58
- 59 (13) Ockwig, N. W.; Delgado-Friedrichs, O.; O’Keeffe, M.; Yaghi, O. M. Reticular
60 Chemistry: Occurrence and Taxonomy of Nets and Grammar for the Design of
Frameworks. *Acc. Chem. Res.* **2005**, *38* (3), 176–182.

- 1
2
3
4
5
6
7
8
9
10
11
12
13
14
15
16
17
18
19
20
21
22
23
24
25
26
27
28
29
30
31
32
33
34
35
36
37
38
39
40
41
42
43
44
45
46
47
48
49
50
51
52
53
54
55
56
57
58
59
60
- (14) O’Keeffe, M.; Yaghi, O. M. Deconstructing the Crystal Structures of Metal-Organic Frameworks and Related Materials into Their Underlying Nets. *Chem. Rev.* **2012**, *112* (2), 675–702.
- (15) Rosi, N. L.; Eckert, J.; Eddaoudi, M.; Vodak, D. T.; Kim, J.; O’Keeffe, M.; Yaghi, O. M. Hydrogen Storage in Microporous Metal-Organic Frameworks. *Science* **2003**, *300* (5622), 1127–1129.
- (16) Tranchemontagne, D. J.; Mendoza-Cortés, J. L.; O’Keeffe, M.; Yaghi, O. M. Secondary Building Units, Nets and Bonding in the Chemistry of Metal-Organic Frameworks. *Chem. Soc. Rev.* **2009**, *38* (5), 1257–1283.
- (17) Wong-Foy, A. G.; Matzger, A. J.; Yaghi, O. M. Exceptional H₂ Saturation Uptake in Microporous Metal-Organic Frameworks. *J. Am. Chem. Soc.* **2006**, *128* (11), 3494–3495.
- (18) Menon, V.; Komarneni, S. Porous Adsorbents for Vehicular Natural Gas Storage: A Review. *J. Porous Mater.* **1998**, *58*, 43–58.
- (19) Rowsell, J. L. C.; Yaghi, O. M. Strategies for Hydrogen Storage in Metal-Organic Frameworks. *Angew. Chem. Int. Ed. Engl.* **2005**, *44* (30), 4670–4679.
- (20) Wang, B.; Côté, A. P.; Furukawa, H.; O’Keeffe, M.; Yaghi, O. M. Colossal Cages in Zeolitic Imidazolate Frameworks as Selective Carbon Dioxide Reservoirs. *Nature* **2008**, *453* (7192), 207–211.
- (21) Luebbers, M. T.; Wu, T.; Shen, L.; Masel, R. I. Trends in the Adsorption of Volatile Organic Compounds in a Large-Pore Metal-Organic Framework, IRMOF-1. *Langmuir* **2010**, *26* (13), 11319–11329.
- (22) Yang, K.; Sun, Q.; Xue, F.; Lin, D. Adsorption of Volatile Organic Compounds by Metal-Organic Frameworks MIL-101: Influence of Molecular Size and Shape. *J. Hazard. Mater.* **2011**, *195*, 124–131.
- (23) Côté, A. P.; Benin, A. I.; Ockwig, N. W.; O’Keeffe, M.; Matzger, A. J.; Yaghi, O. M. Porous, Crystalline, Covalent Organic Frameworks. *Science* **2005**, *310* (5751), 1166–1170.
- (24) Ewing, R. C. The Design and Evaluation of Nuclear-Waste Forms: Clues from Mineralogy. *Can. Mineral.* **2001**, *39* (June), 697–715.
- (25) Hamdi, B.; Houari, M.; Hamoudi, S.; Kessaïssia, Z. Adsorption of Some Volatile Organic Compounds on Geomaterials. *Desalination* **2004**, *166*, 449–455.
- (26) Anurova, N.; Blatov, V.; Ilyushin, G.; Blatova, O.; Ivanovschitz, a; Demyanets, L. Migration Maps of Li⁺ Cations in Oxygen-Containing Compounds. *Solid State Ionics* **2008**, *179* (39), 2248–2254.

- 1
2
3 (27) Blatov, V. A. Nanocluster Analysis of Intermetallic Structures with the Program
4 Package TOPOS. *Struct. Chem.* **2012**, *23* (4), 955–963.
5
6
7 (28) Pöyry Energy Limited. *The 2007 UK Radioactive Waste Inventory: A Review of the*
8 *Processes Contributing to Radioactive Wastes in the UK*; 2008.
9
10 (29) Griffith, C. S.; Luca, V. Ion-Exchange Properties of Microporous Tungstates. *Chem.*
11 *Mater.* **2004**, *16* (24), 4992–4999.
12
13
14 (30) Forsberg, C. W. Rethinking High-Level Waste Disposal: Separate Disposal of High-
15 Heat Radionuclides (^{90}Sr and ^{137}Cs) Management and Disposal. *Nucl. Technol.* **2008**,
16 *131* (2), 252–268.
17
18
19 (31) Nikolov, I.; Nikolov, V.; Peshev, P. Regions of Phase Crystallization and New Double
20 Tungstates in the System $\text{Na}_2\text{O}-\text{Al}_2\text{O}_3-\text{WO}_3$. *J. Alloys Compd.* **2003**, *351* (1-2), 202–
21 207.
22
23
24 (32) Okada, K.; Morikawa, H.; Marumo, F.; Iwai, S. Disodium Ditungstate. *Acta*
25 *Crystallogr. Sect. B Struct. Crystallogr. Cryst. Chem.* **1975**, *31* (4), 1200–1201.
26
27 (33) Otwinowski, Z.; Minor, W. Processing of X-ray Diffraction Data Collected in
28 Oscillation Mode. In *Methods in Enzymology, Volume 276: Macromolecular*
29 *Crystallography, Part A*, pp307-326; Carter, C. W. Jr., Sweet R. M., Eds.; Academic
30 Press: New York, **1997**.
31
32
33 (34) Blessing, R. H. An Empirical Correction for Absorption Anisotropy. *Acta Crystallogr.*
34 *A.* **1995**, *51* (Pt 1) (1), 33–38.
35
36
37 (35) Rigaku Americas and Rigaku. CrystalClear-SM Expert 2.0 software, **2009**.
38
39 (36) Higashi, T. ABSCOR, Rigaku Corporation, Tokyo, Japan, **1995**.
40
41 (37) Sheldrick, G. M. A Short History of SHELX. *Acta Crystallogr. A.* **2008**, *64* (Pt 1),
42 112–122.
43
44
45 (38) Hautier, G.; Fischer, C.; Ehlacher, V.; Jain, A.; Ceder, G. Data Mined Ionic
46 Substitutions for the Discovery of New Compounds. *Inorg. Chem.* **2011**, *50*, 656–663.
47
48
49 (39) Delgado-Friedrichs, O.; O’Keeffe, M. Crystal Nets as Graphs: Terminology and
50 Definitions. *J. Solid State Chem.* **2005**, *178* (8), 2480–2485.
51
52 (40) Bonneau, C.; Delgado-Friedrichs, O.; O’Keeffe, M.; Yaghi, O. M. Three-Periodic Nets
53 and Tilings: Minimal Nets. *Acta Crystallogr. A.* **2004**, *60* (Pt 6), 517–520.
54
55
56 (41) Blatov, V. A.; O’Keeffe, M.; Proserpio, D. M. Vertex-, Face-, Point-, Schläfli-, and
57 Delaney-Symbols in Nets, Polyhedra and Tilings: Recommended Terminology.
58 *CrystEngComm* **2010**, *12* (1), 44.
59
60

- 1
2
3
4
5
6
7
8
9
10
11
12
13
14
15
16
17
18
19
20
21
22
23
24
25
26
27
28
29
30
31
32
33
34
35
36
37
38
39
40
41
42
43
44
45
46
47
48
49
50
51
52
53
54
55
56
57
58
59
60
- (42) Essam, J. W.; Fisher, M. E. Some Basic Definitions in Graph Theory. *Rev. Mod. Phys.* **1970**, *42* (2), 272–288.
- (43) Blatov, V. A.; Delgado-Friedrichs, O.; O’Keeffe, M.; Proserpio, D. M. Three-Periodic Nets and Tilings: Natural Tilings for Nets. *Acta Crystallogr. A.* **2007**, *63* (Pt 5), 418–425.
- (44) Slater, J. C. Atomic Radii in Crystals. *J. Chem. Phys.* **1964**, *41* (10), 3199.
- (45) Desgranges, L.; Baldinozzi, G.; Rousseau, G.; Nièpce, J.-C.; Calvarin, G. Neutron Diffraction Study of the in Situ Oxidation of UO(2). *Inorg. Chem.* **2009**, *48*, 7585–7592.
- (46) Belin, R. C.; Valenza, P. J.; Reynaud, M. A.; Raison, P. E. New Hermetic Sample Holder for Radioactive Materials Fitting to Siemens D5000 and Bruker D8 X-Ray Diffractometers: Application to the Rietveld Analysis of Plutonium Dioxide. *J. Appl. Crystallogr.* **2004**, *37* (6), 1034–1037.
- (47) Taggard Jr, J. E.; Foord, E. E.; Rosenzweig, A.; Hanson, T. Scrutinyite, Natural Occurrence of A-PbO₂ from Bingham, New Mexico, U.S.A., and Mapimi, Mexico. *Can. Mineral.* **1988**, *26*, 905–910.
- (48) Kolitsch, U.; Maczka, M.; Hanuza, J. NaAl(MoO₄)₂: A Rare Structure Type among Layered Yavapaiite-Related AM(XO₄)₂ Compounds. *Acta Crystallogr. Sect. E Struct. Reports Online* **2003**, *59* (2), i10–i13.
- (49) Sozzani, P.; Bracco, S.; Comotti, A.; Ferretti, L.; Simonutti, R. Methane and Carbon Dioxide Storage in a Porous van Der Waals Crystal. *Angew. Chem. Int. Ed. Engl.* **2005**, *44* (12), 1816–1820.
- (50) Michel, C.; Groult, D.; Deschanvres, A.; Raveau, B. Proprietes D’echange D’ions Des Pyrochlores AB₂O₆—II Evolution Thermique Des Pyrochlores AMWO₆.H₂O (A = Li, Na, Ag; M = Nb, Ta, Sb). *Journal of Inorganic and Nuclear Chemistry*, 1975, *37*, 251–255.
- (51) Knyazev, A. V.; Maczka, M.; Smirnova, N. N.; Macalik, L.; Kuznetsova, N. Y.; Letyanina, I. A. Crystal Structure, Spectroscopy and Thermodynamic Properties of MIVWO₆(MI – Li, Na). *J. Solid State Chem.*, **2009**, *182*, 3003–3012.
- (52) Berdonosov, P. S.; Charkin, D. O.; Knight, K. S.; Johnston, K. E.; Goff, R. J.; Dolgikh, V. A.; Lightfoot, P. Phase Relations and Crystal Structures in the Systems (Bi,Ln)₂WO₆ and (Bi,Ln)₂MoO₆ (Ln=lanthanide). *J. Solid State Chem.* **2006**, *179*, 3437–3444.
- (53) Macalik, L.; Tomaszewski, P. E.; Lisiecki, R.; Hanuza, J. The Crystal Structure, Vibrational and Luminescence Properties of the Nanocrystalline KEu(WO₄)₂ and KGd(WO₄)₂:Eu³⁺ Obtained by the Pechini Method. *J. Solid State Chem.*, **2008**, *181*, 2591–2600.

- 1
2
3
4
5
6
7
8
9
10
11
12
13
14
15
16
17
18
19
20
21
22
23
24
25
26
27
28
29
30
31
32
33
34
35
36
37
38
39
40
41
42
43
44
45
46
47
48
49
50
51
52
53
54
55
56
57
58
59
60
- (54) Fu, W. T.; Au, Y. S.; Akerboom, S.; IJdo, D. J. W. Crystal Structures and Chemistry of Double Perovskites $Ba_2M(II)M'(VI)O_6$ ($M=Ca, Sr, M'=Te, W, U$). *J. Solid State Chem.* **2008**, *181*, 2523–2529.
- (55) Krut'ko, V. A.; Belik, A. A.; Lysanova, G. V. Structures of Nonlinear Hexagonal Boratungstates $Ln_3 B W O_9$ ($Ln= La, Pr, Nd, Sm, Gd, Tb, Dy$). *Zhurnal Neorg. Khimii* **2006**, *51* (6), 954–959.
- (56) Hong, S. T. Novel Perovskite-Related Barium Tungstate $Ba_{11}W_4O_{23}$. *J. Solid State Chem.* **2007**, *180*, 3039–3048.
- (57) Lv, P.; Chen, D.; Li, W.; Xue, L.; Huang, F.; Liang, J. Subsolidus Phase Relationships in the System $ZnO-Li_2O-WO_3$. *J. Alloys Compd.* **2008**, *460*, 142–146.
- (58) Jiang, H. L.; En, M.; Mao, J. G. New Luminescent Solids in the $Ln-W(Mo)-Te-O(Cl)$ Systems. *Inorg. Chem.* **2007**, *46* (17), 7012–7023.
- (59) Brixner, L. H.; Chen, H. -y.; Foris, C. M. Structure and Luminescence of the Monoclinic $LnWO_4Cl$ -Type Rare Earth Halo Tungstates. *Mater. Res. Bull.* **1982**, *17*, 1545–1556.
- (60) Boulahya, K.; Parras, M.; González-Calbet, J. M. A Structural Study of the Solid Solution $Eu_2(Mo_{1-x}W_x)_3O_{12}$. *Z. Anorg. Allg. Chem.* **2005**, *631*, 1988–1990.
- (61) Bang Jin, G.; Soderholm, L. Syntheses and Single-Crystal Structures of $CsTh(MoO_4)_2Cl$ and $Na_4Th(WO_4)_4$. *J. Solid State Chem.* **2011**, *184*, 337–342.
- (62) Efremov, V. A.; Berezina, T. A.; Averina, I. M.; Trunov, V. K. Structure of $Na_5 Tb (Mo O_4)_4$, $Na_5 Lu (Mo O_4)_4$, and $Na_5 Lu (W O_4)_4$. *Kristallografiya* **1980**, *25*, 254–261.
- (63) Efremov, V. A.; Trunov, V. K.; Berezina, T. A. Fine Changes in the Structure of Scheelite-like $Na_5 Tr (E O_4)_4$ with a Variation in Their Elemental Composition. *Kristallografiya* **1982**, *27*, 134–139.
- (64) Grivel, J. C.; Norby, P. Subsolidus Phase Relations of the $SrO-WO_3-CuO$ System at $800^\circ C$ in Air. *J. Alloys Compd.* **2012**, *513*, 304–309.
- (65) Manjón, F. J.; López-Solano, J.; Ray, S.; Gomis, O.; Santamaría-Pérez, D.; Mollar, M.; Panchal, V.; Errandonea, D.; Rodríguez-Hernández, P.; Muñoz, A. High-Pressure Structural and Lattice Dynamical Study of $HgWO_4$. *Phys. Rev. B - Condens. Matter Mater. Phys.* **2010**, *82*, 035212–1 – 035212–12.
- (66) Klug, A. X-Ray Diffraction Studies of Potassium Polytungstates with High WO_3 Content. *Mater. Res. Bull.*, **1977**, *12*, 837–845.
- (67) Okada, K.; Marumo, F.; Iwai, S. The Crystal Structure of $K_2W_4O_{13}$. *Acta Crystallogr. Sect. B Struct. Crystallogr. Cryst. Chem.* **1978**, *34*, 3193–3195.

- 1
2
3
4
5
6
7
8
9
10
11
12
13
14
15
16
17
18
19
20
21
22
23
24
25
26
27
28
29
30
31
32
33
34
35
36
37
38
39
40
41
42
43
44
45
46
47
48
49
50
51
52
53
54
55
56
57
58
59
60
- (68) Mormann, T. J.; Jeitschko, W. Mercury(I) Molybdates and Tungstates: Hg_2WO_4 and Two Modifications of Hg_2MoO_4 . *Inorg. Chem.* **2000**, *39*, 4219–4223.
- (69) Kovba, L. M.; Lykova, L. N.; Balashov, V. L.; Kharlanov, A. L. Crystal Structure of Ba_2WO_5 . *Koord. Khimiya* **1985**, *11* (10), 1426–1429.
- (70) Guarnieri, A. A.; Moreira, A. M.; Pinheiro, C. B.; Speziali, N. L. Structural and Calorimetric Studies of Mixed $\text{K}_2\text{MoxW}(1-x)\text{O}_4$ ($0 \leq x \leq 1$) Compounds. *Physica B: Condens. Matter*, **2003**, *334*, 303–309.
- (71) Okada, K.; Morikawa, H.; Marumo, F.; Iwai, S. The Crystal Structure of $\text{Li}_2\text{W}_2\text{O}_7$. *Acta Crystallogr. Sect. B Struct. Crystallogr. Cryst. Chem.* **1975**, *31*, 1451–1454.
- (72) Li, Y.-Y.; Cheng, W.-D.; Zhang, H.; Lin, C.-S.; Zhang, W.-L.; Geng, L.; Chai, G.-L.; Luo, Z.-Z.; He, Z.-Z. A Series of Novel Rare-Earth Bismuth Tungstate Compounds LnBiW_2O_9 ($\text{Ln}=\text{Ce}, \text{Sm}, \text{Eu}, \text{Er}$): Synthesis, Crystal Structure, Optical and Electronic Properties. *Dalton Trans.* **2011**, *40*, 7357–7364.
- (73) Hartenbach, I.; Schleid, T. $\text{Na}_3\text{F}[\text{WO}_4]$: A Sodium Fluoride Ortho-Oxotungstate(VI) with Strands of Face-Shared Fluoride-Centred Sodium Octahedra According to. *Z. Anorg. Allg. Chem.* **2007**, *633*, 524–526.
- (74) Hartenbach, I.; Marchetti, B.; Schleid, T. $\text{Na}_5\text{Y}[\text{WO}_4]_4$: Ein Natrium - Yttrium - Ortho-Oxowolframat Mit Einer Teraedrischen Na^+ - Koordination. *Z. Kristallogr. Suppl. Issue* **2007**, *25* (079), 22.
- (75) Sundberg, M.; Marinder, B. Ordered and Defect Structures in the $\text{UO}_2 - \text{WO}_3$ System, Revealed by HREM. *J. Solid State Chem.* **1996**, *121*, 167–173.
- (76) Marinder, B. O.; Wang, P.-L.; Werner, P. E.; Westdahl, M.; Andresen, A. F.; Louer, D. Powder Diffraction Studies of Cu_2WO_4 . *Acta Chem. Scand. Ser. A* **1987**, *41*, 152–157.
- (77) Grice, J. D.; Dunn, P. J. Crystal Structure Determination of Pinalite. *Am. Mineral.* **2000**, *85*, 806–809.
- (78) Müller-Buschbaum, H.; Gressling, T. Zur Dimorphie von Kupfer-Lanthanoid-Oxowolframat Am Beispiel von CuErW_2O_8 , Mit Einem Beitrag Über CuDyW_2O_8 . *J. Alloys Compd.* **1993**, *202*, 63–67.
- (79) Boehlke, A.; Müller-Buschbaum, H. Ein Beitrag Zur Kristallstruktur von CuLaW_2O_8 Und CuSmW_2O_8 . *J. Less Common Met.* **1990**, *162*, 141–147.
- (80) Okada, K.; Ossaka, J.; Iwai, S. Structure of Dithallium tungstate(VI). *Acta Crystallogr. Sect. B Struct. Crystallogr. Cryst. Chem.* **1979**, *35*, 2189–2191.
- (81) Barker, R. S.; Evans, I. R. Structural Characterization of $\text{RE}_{10}\text{W}_{22}\text{O}_{81}$ Rare-Earth Tungstates ($\text{RE} = \text{Ce}, \text{Nd}$). *Acta Crystallogr. Sect. B Struct. Sci.* **2008**, *64*, 708–712.

- 1
2
3
4
5
6
7
8
9
10
11
12
13
14
15
16
17
18
19
20
21
22
23
24
25
26
27
28
29
30
31
32
33
34
35
36
37
38
39
40
41
42
43
44
45
46
47
48
49
50
51
52
53
54
55
56
57
58
59
60
- (82) Mumm, H.-C.; Müller-Buschbaum, H. Zur Kristallstruktur von Cu_2WO_4 . *J. Less Common Met.* **1988**, *142*, 85–90.
- (83) Gressling, T.; Müller-Buschbaum, H. Ein Neuer Strukturtyp Am Lanthanoid-Oxowolframat $\text{FeCe}(\text{WO}_4)\text{W}_2\text{O}_8 = \text{FeCe}(\text{WO}_4)_3$. *Z. Anorg. Allg. Chem.* **1996**, *622*, 254–258.
- (84) Sundberg, M.; Lundberg, M. $\text{K}_x(\text{Nb,W})_{17}\text{O}_{47}$ (1LxL2): A New Tunnel Structure Derived from High-Resolution Electron Micrographs. *Acta Crystallogr. Sect. B Struct. Sci.* **1987**, *43*, 429–434.
- (85) Hanuza, J.; Maczka, M.; Hermanowicz, K.; Andruszkiewicz, M.; Pietraszko, A.; Streck, W.; Dereń, P. The Structure and Spectroscopic Properties of $\text{Al}_{2-x}\text{Cr}_x(\text{WO}_4)_3$ Crystals in Orthorhombic and Monoclinic Phases. *J. Solid State Chem.* **1993**, *105*, 49–69.
- (86) Woodcock, D. A.; Lightfoot, P.; Ritter, C. Negative Thermal Expansion in $\text{Y}_2(\text{WO}_4)_3$. *J. Solid State Chem.* **2000**, *149*, 92–98.
- (87) Chan, L. Y. Y.; Geller, S. Crystal Structure and Conductivity of 26-Silver 18-Iodide Tetratungstate, $\text{Ag}_{26}\text{I}_{18}\text{W}_4\text{O}_{16}$. *J. Solid State Chem.* **1977**, *21*, 331–347.
- (88) Evans, J. S. O.; Mary, T. A.; Vogt, T.; Subramanian, M. A.; Sleight, A. W. Negative Thermal Expansion in ZrW_2O_8 and HfW_2O_8 . *Chem. Mat.* **1996**, *8*, 2809–2823.
- (89) Spitsyn, V. I.; Balashov, V. L.; Kharlanov, A. L.; Lykova, L. N.; Kovba, L. M. Crystal Structure of $\text{Ba}_3\text{WO}_5\text{Cl}_2$. *Dokl. Akad. Nauk SSSR* **1985**, *284* (1), 125–127.
- (90) Tyulin, A. V.; Efremov, V. A. Polymorphism of Oxytungstates Tr_2WO_6 . Mechanism of Structural Changes of $\text{Er}_2\text{W}_2\text{O}_6$. *Kristallografiya* **1987**, *32*, 363–370.
- (91) Tyulin, A. V.; Efremov, V. A.; Trunov, V. K. Polymorphism of Oxytungstates TR_2WO_6 . Mechanisms of Structural Changes in Y_2WO_6 . *Kristallografiya* **1989**, *34*, 885–892.
- (92) Tyulin, A. V.; Efremov, V. A. Polymorphism of Oxytungstates Tr_2WO_6 . Analysis of Structural Type II (Gd_2WO_6 and Gd_2MoO_6). Mechanism of Structural Change in $\text{Gd}_2\text{W}_2\text{O}_6$ in the Phase Transition II \leftrightarrow V. *Kristallografiya* **1987**, *32*, 371–377.
- (93) Farrugia, L. J. Sodium Tungstate Dihydrate: A Redetermination. *Acta Crystallogr. Sect. E Struct. Reports Online* **2007**, *63*.
- (94) Ewing, R. C. Nuclear Waste Forms for Actinides. *Proc. Natl. Acad. Sci. U. S. A.* **1999**, *96* (7), 3432–3439.
- (95) Pujol, M. C.; Mateos, X.; Aznar, A.; Solans, X.; Suriñach, S.; Massons, J.; Díaz, F.; Aguiló, M. Structural Redetermination, Thermal Expansion and Refractive Indices of $\text{KLu}(\text{WO}_4)_2$. *J. Appl. Crystallogr.* **2006**, *39*, 230–236.

- 1
2
3
4
5
6
7
8
9
10
11
12
13
14
15
16
17
18
19
20
21
22
23
24
25
26
27
28
29
30
31
32
33
34
35
36
37
38
39
40
41
42
43
44
45
46
47
48
49
50
51
52
53
54
55
56
57
58
59
60
- (96) Pujol, M. C.; Mateos, X.; Solé, R.; Massons, J.; Gavaldà, J.; Solans, X.; Díaz, F.; Aguiló, M. Structure, Crystal Growth and Physical Anisotropy of KYb(WO₄)₂, a New Laser Matrix. *J. Appl. Crystallogr.* **2002**, *35*, 108–112.
- (97) Borowiec, M. T.; Dyakonov, V. P.; Woźniak, K.; Dobrzycki, Ł.; Berkowski, M.; Zubov, E. E.; Michalski, E.; Szewczyk, A.; Gutowska, M. U.; Zayarnyuk, T.; et al. Crystal Structure and Magnetic Properties of Potassium Erbium Double Tungstate KEr(WO₄)₂. *J. Phys. Condens. Matter* **2007**, *19*, 056206.
- (98) Gallucci, E.; Goutaudier, C.; Boulon, G.; Cohen-Adad, M. T.; Mentzen, B. F. Nonstoichiometric KY(WO₄)₂: Crystal Growth, Chemical and Physical Characterization. *J. Cryst. Growth* **2000**, *209*, 895–905.
- (99) Borowiec, M. T.; Dyakonov, V. P.; Wozniak, K.; Dobrzycki, L.; Majchrowski, A.; Michalski, E.; Zubov, E. E.; Khatsko, E. N.; Zayarnyuk, T.; Szewczyk, A.; et al. Crystalline Structure of Potassium Holmium Double Tungstate. *Acta Phys. Pol. A* **2011**, *119* (6), 835–837.
- (100) Gateshki, M.; Igartua, J. M. Second-Order Structural Phase Transition in Sr₂CuWO₆ Double-Perovskite Oxide. *J. Phys. Condens. Matter* **2003**, *15*, 6749–6757.
- (101) Alvarez-Vega, M.; Rodriguez-Carvajal, J.; Reyes-Cardenas, J. G.; Fuentes, A. F.; Amador, U. Synthesis and Characterization of New Double Tungstates Li₂MII(WO₄)₂ (M = Co, Ni, and Cu). *Chem. Mater.* **2001**, *13*, 3871–3875.
- (102) McDowell, N. A.; Knight, K. S.; Lightfoot, P. Unusual High-Temperature Structural Behaviour in Ferroelectric Bi₂WO₆. *Chem. - A Eur. J.* **2006**, *12*, 1493–1499.
- (103) Shen, R.; Wang, C.; Wang, T. M.; Dong, C.; Chen, X. L.; Liang, J. K. Crystal Structures of Dy₂(WO₄)₃ and GdY(WO₄)₃. *Rare Met.* **2003**, *22* (1), 49–54.
- (104) Templeton, D. H.; Zalkin, A. Crystal Structure of Europium Tungstate. *Acta Crystallogr.* **1963**, *16*, 762–766.
- (105) Polyanskaya, T. M.; Borisov, S. V.; Belov, N. V. The Crystal Structure of Pr₃WO₆Cl₃. *Dokl. Akad. Nauk SSSR* **1969**, *187*, 1043–1046.
- (106) Parise, J. B.; Brixner, L. H.; Prince, E. Refinement of the Structure of Trilanthanum Trichlorohexaoxotungstate, La₃WO₆Cl₃, from Neutron Powder Diffraction Data. *Acta Crystallogr. Sect. C Cryst. Struct. Commun.* **1983**, *39*, 1326–1328.
- (107) Michel, C.; Guyomarc'h, A.; Raveau, B. Nouveaux Echangeurs Cationiques Avec Une Structure a Tunnels Entrecroises: Les Oxydes A₁₂M₃₃O₉₀ et A₁₂M₃₃O₉₀, 12H₂O. *J. Solid State Chem.* **1977**, *22*, 393–403.
- (108) Kim, J. S.; Lee, J. C.; Cheon, C. Il; Kang, H. J. Crystal Structures and Low Temperature Cofiring Ceramic Property of (1 - X)(Li, RE)W₂O₈-xBaWO₄ Ceramics (RE = Y, Yb). *Japanese J. Appl. Physics, Part 1 Regul. Pap. Short Notes Rev. Pap.* **2006**, *45*, 7397–7400.

- 1
2
3
4 (109) Kondo, R. The Synthesis and Crystallography of a Group of New Compounds
5 Belonging to the Hauyne Type Structure. *J. Ceram. Assoc. Japan* **1965**, *73*, 1–8.
6
7 (110) Müller-Buschbaum, H.; Sedello, O. Die Kristallstrukturen von A-CuGdW₂O₈ Und
8 CuNdMo₂O₈. *J. Alloys Compd.* **1994**, *204*, 237–241.
9
10 (111) Klevtsova, R. F.; Kharchenko, L. Y.; Borisov, S. V.; Efremov, V. A.; Klevtsov, P. V.
11 Triclinic Modification of Lithium-Rare Earth Tungstates Li Ln (W O₄)₂, Where Ln Is
12 La-Sm. *Kristallografiya* **1979**, *24*, 446–454.
13
14 (112) Gressling, T.; Müller-Buschbaum, H. Ein Neuer Strukturtyp Bei Kupfer-Lanthanoid-
15 Oxowolframaten: CuDy₅(WO₄)₈. *Z. Anorg. Allg. Chem.* **1995**, *621*, 181–185.
16
17 (113) Shigematsu, H.; Nomura, K.; Nishiyama, K.; Tojo, T.; Kawaji, H.; Atake, T.;
18 Kawamura, Y.; Miyoshi, T.; Matsushita, Y.; Tanaka, M.; et al. Structures and Phase
19 Transitions in Rb₂MoO₄ and Rb₂WO₄. *Ferroelectrics* **2011**, *414*, 195–200.
20
21 (114) Chang, H. Y.; Sivakumar, T.; Ok, K. M.; Shiv Halasyamani, P. Polar Hexagonal
22 Tungsten Bronze-Type Oxides: KNbW₂O₉, RbNbW₂O₉, and KTaW₂O₉. *Inorg.*
23 *Chem.* **2008**, *47*, 8511–8517.
24
25 (115) Rozanova, O. N.; Pol'shchikova, Z. Y.; Kovba, L. M. Crystal Structure of Uranium
26 Tungstate U (W O₄)₂. *Radiokhimiya* **1978**, *20*, 125–127.
27
28 (116) Singh, D. J. Relationship of Li₂W O₄ to the Scheelite Tungstate Scintillators:
29 Electronic Structure and Atomic Positions from Density-Functional Calculations.
30 *Phys. Rev. B - Condens. Matter Mater. Phys.* **2008**, *77*, 113101.
31
32 (117) Zachariasen, W. H.; Plettinger, H. A. The Crystal Structure of Lithium Tungstate. *Acta*
33 *Crystallogr.* **1961**, *14*, 229–230.
34
35 (118) Abrahams, S. C.; Bernstein, J. L. Crystal Structure of the Transition-Metal Molybdates
36 and Tungstates. II. Diamagnetic Sc₂(WO₄)₃. *J. Chem. Phys.* **1966**, *45*, 2745–2752.
37
38 (119) Richard, A. P.; Edwards, D. D. Subsolidus Phase Relations and Crystal Structures of
39 the Mixed-Oxide Phases in the In₂O₃-WO₃ System. *J. Solid State Chem.* **2004**, *177*,
40 2740–2748.
41
42 (120) Lamire, M.; Labbé, P.; Goreaud, M.; Raveau, B. Ba₂P₈W₃₂O₁₁₂: Structural Study in
43 Comparison with the K and Rb Diphosphate Tungsten Bronzes with Hexagonal
44 Tunnels. *J. Solid State Chem.* **1987**, *71*, 342–348.
45
46 (121) Chakraborty, K. R.; Das, A.; Krishna, P. S. R.; Yusuf, S. M.; Patwe, S. J.; Achary, S.
47 N.; Tyagi, A. K. A Low Temperature Magnetization and Neutron Diffraction Study of
48 Ca₂NiWO₆. *J. Alloys Compd.* **2008**, *457*, 15–18.
49
50 (122) Horiuchi, H.; Morimoto, N.; Yamaoka, S. The Crystal Structure of Li₂WO₄II: A
51 Structure Related to Spinel. *J. Solid State Chem.* **1979**, *30*, 129–135.
52
53
54
55
56
57
58
59
60

- 1
2
3
4
5
6
7
8
9
10
11
12
13
14
15
16
17
18
19
20
21
22
23
24
25
26
27
28
29
30
31
32
33
34
35
36
37
38
39
40
41
42
43
44
45
46
47
48
49
50
51
52
53
54
55
56
57
58
59
60
- (123) Depmeier, W.; Yamamoto, A. Powder Profile Refinement of a Commensurately Modulated Aluminate Sodalite. *Mater. Sci. Forum* **1991**, 79-82, 763–768.
- (124) Champarnaud-Mesjard, J.-C.; Frit, B.; Watanabe, A. Crystal Structure of Bi₂W₂O₉, the n=2 Member of the Homologous Series (Bi₂O₂)_nBVInO_{3n+1} of Cation-Deficient Aurivillius Phases. *J. Mater. Chem.* **1999**, 9, 1319–1322.
- (125) Jorgensen, J.; Hu, Z.; Teslic, S.; Argyriou, D.; Short, S.; Evans, J.; Sleight, A. Pressure-Induced Cubic-to-Orthorhombic Phase Transition in ZrW₂O₈. *Phys. Rev. B* **1999**, 59, 215–225.
- (126) Okada, K.; Ossaka, J. Caesium Lithium Tungstate: A Stuffed H-Cristobalite Structure. *Acta Crystallogr. Sect. B Struct. Crystallogr. Cryst. Chem.* **1980**, 36, 657–659.
- (127) Wang, K.; Zhang, J.; Wang, J.; Yu, W.; Zhang, H.; Wang, X.; Wang, Z.; Ba, M. Growth, Structure and Morphology Study of Monoclinic RbGd(WO₄)₂ Crystals. *J. Cryst. Growth* **2005**, 281, 407–410.
- (128) Xie, H.; Shen, D.; Xie, C.; Wang, X.; Shen, G. Crystal Growth and Structure of KBi(WO₄)₂ Single Crystals. *Cryst. Res. Technol.* **2006**, 41, 961–966.
- (129) Borowiec, M. T.; Prokhorov, A. D.; Krygin, I. M.; Dyakonov, V. P.; Woźniak, K.; Dobrzycki; Zayarnyuk, T.; Barański, M.; Domuchowski, W.; Szymczak, H. Crystal Structure and EPR of the RbNd(WO₄)₂ Single Crystal. *Phys. B Condens. Matter* **2006**, 371, 205–209.
- (130) Obbade, S.; Dion, C.; Bekaert, E.; Yagoubi, S.; Saadi, M.; Abraham, F. Synthesis and Crystal Structure of New Uranyl Tungstates M₂(UO₂)(W₂O₈) (M=Na, K), M₂(UO₂)₂(WO₅)O (M=K, Rb), and Na₁₀(UO₂)₈(W₅O₂₀)O₈. *J. Solid State Chem.* **2003**, 172, 305–318.
- (131) Obbade, S.; Yagoubi, S.; Dion, C.; Saadi, M.; Abraham, F. Two New Lithium Uranyl Tungstates Li₂(UO₂)(WO₄)₂ and Li₂(UO₂)₄(WO₄)₄O with Framework Based on the Uranophane Sheet Anion Topology. *J. Solid State Chem.* **2004**, 177, 1681–1694.
- (132) Horiuchi, H.; Morimoto, N.; Yamaoka, S. The Crystal Structure of Li₂WO₄(IV) and Its Relation to the Wolframite-Type Structure. *J. Solid State Chem.* **1980**, 33, 115–119.
- (133) Huang, J.; Xu, J.; Li, H.; Luo, H.; Yu, X.; Li, Y. Determining the Structure of Tetragonal Y₂WO₆ and the Site Occupation of Eu³⁺ Dopant. *J. Solid State Chem.* **2011**, 184 (4), 843–847.
- (134) Stomberg, R. Structure of Potassium tetraperoxotungstate(VI), K₂[W(O₂)₄]. *J. Less Common Met.* **1988**, 143, 363–371.
- (135) Depmeier, W. Structure of Cubic Aluminate Sodalite Ca₈[Al₁₂O₂₄](WO₄)₂ in Comparison with Its Orthorhombic Phase and with Cubic Sr₈[Al₁₂O₂₄](CrO₄)₂. *Acta Crystallogr. Sect. B Struct. Sci.* **1988**, 44, 201–207.

- 1
2
3
4 (136) Knight, K. S. The Crystal Structure of Russellite; a Re-Determination Using Neutron
5 Powder Diffraction of Synthetic Bi₂WO₆. *Mineral. Mag.* **1992**, *56*, 399–409.
6
7 (137) Gärtner, M.; Abeln, D.; Pring, A.; Wilde, M.; Reller, A. Synthesis, Structure, and
8 Reactivity of Novel Lanthanum Tungstates. *J. Solid State Chem.* **1994**, *111*, 128–133.
9
10 (138) Jeannin, Y.; Launay, J. P.; Sedjadi, M. A. S. Crystal and Molecular Structure of the
11 Six-Electron-Reduced Form of Metatungstate Rb₄H₈[H₂W₁₂O₄₀](H₂O)₁₈:
12 Occurrence of a Metal-Metal Bonded Subcluster in a Heteropolyanion Framework.
13 *Inorg. Chem.* **1980**, *19*, 2933–2935.
14
15 (139) Fourquet, J. L.; Le Bail, A.; Gillet, P. A. LiNbWO₆: Crystal Structure of Its Two
16 Allotropic Forms. *Mater. Res. Bull.* **1988**, *23*, 1163–1170.
17
18 (140) Knyazev, A. V.; McZka, M.; Kuznetsova, N. Y. Thermodynamic Modeling, Structural
19 and Spectroscopic Studies of the KNbWO₆-KSbWO₆-KTaWO₆ System.
20 *Thermochim. Acta* **2010**, *506*, 20–27.
21
22 (141) Knyazev, A. V.; Kuznetsova, N. Y. Crystal Structure of Compounds CsAV₂VI₂O₆
23 (AV = Sb, Ta; A'VI = W, U). *Radiochemistry* **2009**, *51*, 1–4.
24
25 (142) Murphy, D.; Cava, R.; Rhyne, K.; Roth, R.; Santoro, A.; Zahurak, S.; Dye, J.
26 Structural Aspects of Insertion Reactions of the Pyrochlore, KNbWO₆. *Solid State*
27 *Ionics* **1986**, *18-19*, 799–801.
28
29 (143) Pakhomov, V. I.; Fedorov, P. M.; Okunera, A. S.; Sorokina, O. V. Structure and
30 Elastic Properties of AgIn(WO₄)₂. *Koord. Khimiya* **1977**, *3*, 765–767.
31
32 (144) Postema, J. M.; Fu, W. T.; Ijdo, D. J. W. Crystal Structure of LiLnW₂O₈
33 (Ln=lanthanides and Y): An X-Ray Powder Diffraction Study. *J. Solid State Chem.*
34 **2011**, *184* (8), 2004–2008.
35
36 (145) Tyagi, M.; Singh, S. G.; Sangeeta; Prasad, R.; Auluck, S.; Singh, D. J. A Study of
37 Electronic and Optical Properties of NaBi(WO₄)₂: A Disordered Double Tungstate
38 Crystal. *Phys. B Condens. Matter* **2010**, *405*, 3267–3271.
39
40 (146) Bonin, M.; Paciorek, W.; Schenk, K. J.; Chapuis, G. X-Ray Study of and Structural
41 Approach to the Incommensurate Perovskite Pb₂CoWO₆. *Acta Crystallogr. Sect. B*
42 *Struct. Sci.* **1995**, *51*, 48–54.
43
44 (147) Zhengmin, F.; Wenxiu, L. Crystal Structure of the High-Temperature Phase of a
45 Compound Sr₂ZnWO₆. *Powder Diffr.* **1992**, *7*, 226–227.
46
47 (148) Patwe, S. J.; Achary, S. N.; Mathews, M. D.; Tyagi, A. K. Synthesis, Phase Transition
48 and Thermal Expansion Studies on M₂MgWO₆ (M = Ba²⁺ and Sr²⁺) Double
49 Perovskites. *J. Alloys Compd.* **2005**, *390*, 100–105.
50
51
52
53
54
55
56
57
58
59
60

- 1
2
3
4
5
6
7
8
9
10
11
12
13
14
15
16
17
18
19
20
21
22
23
24
25
26
27
28
29
30
31
32
33
34
35
36
37
38
39
40
41
42
43
44
45
46
47
48
49
50
51
52
53
54
55
56
57
58
59
60
- (149) Martínez-Lope, M. J.; Alonso, J. A.; Casais, M. T.; Fernández-Díaz, M. T. Preparation, Crystal and Magnetic Structure of the Double Perovskites Ba₂CoBO₆ (B = Mo, W). *Eur. J. Inorg. Chem.* **2002**, 2002, 2463–2469.
- (150) Cox, D. E.; Shirane, G.; Frazer, B. C. Neutron-Diffraction Study of Antiferromagnetic Ba₂CoWO₆ and Ba₂NiWO₆. *J. Appl. Phys.* **1967**, 38, 1459–1460.
- (151) Azad, A. K.; Eriksson, S.-G.; Mellergård, A.; Ivanov, S. A.; Eriksen, J.; Rundlöf, H. A Study on the Nuclear and Magnetic Structure of the Double Perovskites A₂FeWO₆ (A = Sr, Ba) by Neutron Powder Diffraction and Reverse Monte Carlo Modeling. *Mater. Res. Bull.* **2002**, 37, 1797–1813.
- (152) Baldinozzi, G.; Sciau, P.; Buffat, P.-A. Investigation of the Orthorhombic Structures of Pb₂MgWO₆ and Pb₂CoWO₆. *Solid State Commun.* **1993**, 86 (9), 541–544.
- (153) Bugaris, D. E.; Hodges, J. P.; Huq, A.; zur Loye, H.-C. Crystal Growth, Structures, and Optical Properties of the Cubic Double Perovskites Ba₂MgWO₆ and Ba₂ZnWO₆. *J. Solid State Chem.* **2011**, 184 (8), 2293–2298.
- (154) Fu, W. T.; Akerboom, S.; IJdo, D. J. W. Crystal Structures of the Double Perovskites Ba₂Sr_{1-x}CaxWO₆. *J. Solid State Chem.* **2007**, 180 (5), 1547–1552.
- (155) Klevtsov, P. V.; Klevtsova, R. F. Single-Crystal Synthesis and Investigation of the Double Tungstates NaR₃+(WO₄)₂, Where R₃⁺ = Fe, Sc, Ga, and In. *J. Solid State Chem.* **1970**, 2, 278–282.
- (156) Keeling, R. O. The Structure of NiWO₄. *Acta Crystallogr.* **1957**, 10, 209–213.
- (157) Shimony, Y.; Ben-Dor, L. On the Crystal Structure of CrWO₄. *Mater. Res. Bull.* **1983**, 18, 331–335.
- (158) Errandonea, D.; Pellicer-Porres, J.; Manjón, F. J.; Segura, A.; Ferrer-Roca, C.; Kumar, R. S.; Tschauer, O.; Rodríguez-Hernández, P.; López-Solano, J.; Radescu, S.; et al. High-Pressure Structural Study of the Scheelite Tungstates CaWO₄ and SrWO₄. *Phys. Rev. B - Condens. Matter Mater. Phys.* **2005**, 72, 174106.
- (159) Velikodnyi, Y. A.; Trunov, V. K. Structure of the Double Wolframate Na In (W O₄)₂. *Zhurnal Strukt. Khimii* **1971**, 12, 334.
- (160) Errandonea, D.; Pellicer-Porres, J.; Manjón, F. J.; Segura, A.; Ferrer-Roca, C.; Kumar, R. S.; Tschauer, O.; López-Solano, J.; Rodríguez-Hernández, P.; Radescu, S.; et al. Determination of the High-Pressure Crystal Structure of BaWO₄ and PbWO₄. *Phys. Rev. B - Condens. Matter Mater. Phys.* **2006**, 73, 224103.
- (161) Baldinozzi, G.; Sciau, P.; Lapasset, J. Crystal Structure of Pb₂CoWO₆ in the Cubic Phase. *Phys. Status Solidi* **1992**, 133, 17–23.
- (162) Becka, L. N.; Poljak, R. . Estructura Cristalina Del MoO₄Na₂ Y Del WO₄Na₂. *An. la Asoc. Quim. Argentina* **1958**, 46, 204–209.

- 1
2
3 (163) Cheviré, F.; Tessier, F.; Marchand, R. New Scheelite-Type Oxynitrides in Systems
4 RWO₃N-AWO₄ (R = Rare-Earth Element; A = Ca, Sr) from Precursors Obtained by
5 the Citrate Route. *Mater. Res. Bull.* **2004**, *39*, 1091–1101.
6
7
8 (164) Zhao, D.; Li, F.; Cheng, W.; Zhang, H. Scheelite-Type NaDy(WO₄)₂. *Acta*
9 *Crystallogr. Sect. E Struct. Reports Online* **2010**, *66*.
10
11 (165) Hanuza, J.; Benzar, A.; Haznar, A.; Maczka, M.; Pietraszko, A.; Van Der Maas, J. H.
12 Structure and Vibrational Dynamics of Tetragonal NaBi(WO₄)₂ Scheelite Crystal.
13 *Vib. Spectrosc.* **1996**, *12*, 25–36.
14
15 (166) Li, H.; Hong, G.; Yue, S. Crystal Study of NaLn(WO₄)₂ (Ln= La, Pr, Nd). *Zhongguo*
16 *Xitu Xuebao* **1990**, *8*, 37–41.
17
18 (167) Perets, S.; Tseitlin, M.; Shneck, R. Z.; Mogilyanski, D.; Kimmel, G.; Burshtein, Z.
19 Sodium Gadolinium Tungstate NaGd(WO₄)₂: Growth, Crystallography, and Some
20 Physical Properties. *J. Cryst. Growth* **2007**, *305*, 257–264.
21
22 (168) Xu, K.-Q.; Xue, J.-Y.; Ding, Y.; Lu, G.-G. Discovery of Stolzite in China and
23 Refinement of Its Crystal Structure. *Dizhi Xuebao* **1994**, *68*, 287–292.
24
25 (169) De Moraes, J. R.; Baldochi, S. L.; Soares, L. dos R. L.; Mazzocchi, V. L.; Parente, C.
26 B. R.; Courrol, L. C. Growth, Structural and Optical Characterizations of
27 LiLa(1-x)Eux(WO₄)₂ Single-Crystalline Fibers by the Micro-Pulling-down Method.
28 *Mater. Res. Bull.* **2012**, *47*, 744–749.
29
30 (170) Klevtsova, R. F.; Bakakin, V. V.; Solodovnikov, S. F.; Glinskaya, L. A. The
31 Combination of the Wolframite's and Scheelite's Motives in the Crystal Structure of
32 Sodium and Zirconium Tungstate Na₂ZrW₃O₁₂ = Na₂ZrW₂O₈(WO₄). *Zhurnal*
33 *Strukt. Khimii* **1981**, *22*, 6–11.
34
35 (171) Gokhman, L. Z.; Dzhurinskii, B. F.; Efremov, V. A.; Ilyukhin, A. B.; Chistova, V. I.
36 Synthesis and Structure of Boratotungstates Ln₃ B W O₉ (Ln= La, Pr, Nd, Sm-Ho).
37 *Zhurnal Neorg. Khimii* **1994**, *39*, 1075–1079.
38
39 (172) Han, X.; Lin, Z.; Hu, Z.; Wang, G. Structure of KLa(WO₄)₂ with a Novel Isolated La
40 Polyhedron. *Mater. Res. Innov.* **2002**, *6*, 118–121.
41
42 (173) Torardi, C. C.; Page, C.; Brixner, L. H.; Blasse, G.; Dirksen, G. J. Structure and
43 Luminescence of Some CsLnW₂O₈ Compounds. *J. Solid State Chem.* **1987**, *69*, 171–
44 178.
45
46 (174) Ra, H. S.; Ok, K. M.; Halasyamani, P. S. Combining Second-Order Jahn-Teller
47 Distorted Cations to Create Highly Efficient SHG Materials: Synthesis,
48 Characterization, and NLO Properties of BaTeM₂O₉ (M = Mo⁶⁺ or W⁶⁺). *J. Am.*
49 *Chem. Soc.* **2003**, *125*, 7764–7765.
50
51
52
53
54
55
56
57
58
59
60

- 1
2
3
4
5
6
7
8
9
10
11
12
13
14
15
16
17
18
19
20
21
22
23
24
25
26
27
28
29
30
31
32
33
34
35
36
37
38
39
40
41
42
43
44
45
46
47
48
49
50
51
52
53
54
55
56
57
58
59
60
- (175) Mączka, M.; Tomaszewski, P.; Stępień-Damm, J.; Majchrowski, A.; Macalik, L.; Hanuza, J. Crystal Structure and Vibrational Properties of Nonlinear Eu₃BWO₉ and Nd₃BWO₉ Crystals. *J. Solid State Chem.* **2004**, *177*, 3595–3602.
- (176) Goodey, J.; Ok, K. M.; Broussard, J.; Hofmann, C.; Escobedo, F. V.; Halasyamani, P. S. Syntheses, Structures, and Second-Harmonic Generating Properties in New Quaternary Tellurites: A₂TeW₃O₁₂ (A=K, Rb, or Cs). *J. Solid State Chem.* **2003**, *175*, 3–12.
- (177) Range, K.-J.; Klement, U.; Rau, F.; Schiessl, U.; Heyns, A. M. Crystal Structure of Rubidium ditungstate(VI), Rb₂W₂O₇. *Z. Kristallogr.* **1993**, *203*, 318–319.
- (178) Moutou, J. M.; Vlasse, M.; Cervera-Marzal, M.; Chaminade, J. P.; Pouchard, M. A Structural Study of a New Lithium Oxyfluorotungstate, LiW₃O₉F. *J. Solid State Chem.* **1984**, *51*, 190–195.
- (179) Hong, H. -P.; Dwight, K. Crystal Structure and Fluorescence Lifetime of a Laser Material NdNa₅(WO₄)₄. *Mater. Res. Bull.* **1974**, *9*, 775–780.
- (180) Klevtsova, R. F.; Volkova, L. M. Crystal Structure of Monoclinic K Nd (W O₄)₂. *Kristallografiya* **1972**, *17*, 859–861.
- (181) Zikmund, Z. The Crystal Structure of Ca₃WO₆Cl₂ and the Configuration of the WO₅₄- Ion. *Acta Crystallogr. Sect. B Struct. Crystallogr. Cryst. Chem.* **1974**, *30*, 2587–2593.
- (182) Klevtsova, R. F.; Borisov, S. V. The Crystal Structure of NdWO₄(OH). *Kristallografiya* **1969**, *14*, 904–907.
- (183) Li, J.; Pan, S.; Zhao, W.; Tian, X.; Han, J.; Fan, X. Synthesis and Crystal Structure of a Novel Boratotungstate: Pb₆B₂WO₁₂. *Solid State Sci.* **2011**, *13*, 966–969.
- (184) Bruedgam, I.; Fuchs, J.; Hartl, H.; Palm, R. Two New isopolyoxotungstates(VI) with the Empirical Composition Cs₂W₂O₇ * 2(H₂O) and Na₂W₂O₇ * H₂O: A Icosatetratungstate and a Polymeric Compound. *Angew. Chemie. Int. Ed.* **1998**, *37*, 2668–2671.
- (185) Meredig, B.; Wolverton, C. A Hybrid Computational-Experimental Approach for Automated Crystal Structure Solution. *Nat. Mater.* **2013**, *12*, 123–127.
- (186) Yang, L.; Dacek, S.; Ceder, G. Proposed Definition of Crystal Substructure and Substructural Similarity. *Phys. Rev. B - Condens. Matter Mater. Phys.* **2014**, *90* (5), 1–9.
- (187) Fuchs, A. H.; Cheetham, A. K. Adsorption of Guest Molecules in Zeolitic Materials: Computational Aspects. *J. Phys. Chem. B* **2001**, *105* (31), 7375–7383.

- 1
2
3 (188) Akten, E. D.; Siriwardane, R.; Sholl, D. S. Monte Carlo Simulation of Single- and
4 Binary-Component Adsorption of CO₂, N₂, and H₂ in Zeolite Na-4A. *Energy & Fuels*
5 **2003**, *17* (7), 977–983.
6
7
8 (189) Corma, A.; Garcia, H. Supramolecular Host-Guest Systems in Zeolites Prepared by
9 Ship-in-a-Bottle Synthesis. *Eur. J. Inorg. Chem.* **2004**, 1143–1164.
10
11 (190) Ravoo, B. J. Nanofabrication with Metal Containing Dendrimers. *Dalton Trans.* **2008**,
12 No. C, 1533–1537.
13
14
15
16
17
18
19
20
21
22
23
24
25
26
27
28
29
30
31
32
33
34
35
36
37
38
39
40
41
42
43
44
45
46
47
48
49
50
51
52
53
54
55
56
57
58
59
60

Table of Contents Entry

A Topological Analysis of Void Spaces in Tungstate Frameworks: Assessing Storage Properties for the Environmentally Important Guest Molecules and Ions: CO_2 , UO_2 , PuO_2 , U , Pu , Sr^{2+} , Cs^+ , CH_4 , and H_2

By Jacqueline M. Cole, Alisha J. Cramer and Anita Zeidler

Synopsis: Topological analysis is employed to match the size and shape of voids (white) within tungstate host structures (blue) to that of environmentally important guest molecules, atoms or ions, which need a storage medium.

